Received: 16 October 2023 | Revised: 14 January 2024 | Accepted: 20 January 2024

DOI: 10.1002/nme.7442

RESEARCH ARTICLE

WILEY

Some remarks on load modeling in nonlinear structural analysis–Statics with large deformations–Consistent treatment of follower load effects and load control

Karl Schweizerhof | **Alexander Konyukhov**

Institut für Mechanik, Karlsruhe Institute of Technology KIT, Karlsruhe, Germany

Correspondence
Karl Schweizerhof, Institut für Mechanik, Karlsruhe Institute of Technology KIT, Karlsruhe, Germany.
Email: karl.schweizerhof@kit.edu

Abstract

Load modeling in nonlinear statics, particularly incorporating large deformations differs significantly from the treatment in linear analysis. As in structural dynamics masses in a gravity field generate the loading, their location, and their modifications within the deformation process must be considered in a nonlinear simulation. A specific view besides loading by masses is on gas and fluid interaction with structures. In addition, load control using specifically designed algorithms is evaluated with respect to realistic applications. Within the load modeling an unavoidable, however side aspect, is the general discussion about the so-called follower forces and non-conservative loading. As an example of real-world applications, the specifics of inflated rubber dams are presented.

KEYWORDS

arc-length schemes, consistent load control, deformation dependent loading, follower loads, load modeling, nonlinear static analysis, rubber dams

1 | INTRODUCTION AND GOAL OF THE CONTRIBUTION

In structural mechanics, the definition and modeling of static loading for linear cases are well-established. However, in nonlinear mechanics, the situation is often unclear. This raises the following questions:

a) Origin of loading?
b) Loading modification during deformation?
c) General control of loading–increase or decrease of loading for example, by so-called arc-length schemes?

Under these aspects, the topic of this contribution may seem rather old-fashioned, but modern methods such as finite elements and combined with any kind of constrained methods allow many types and combinations of loading of structures. As a consequence, the wide range of modeling choices is very seductive to perform analyses–particularly for highly nonlinear behavior–with often questionable boundary conditions. In standard text books on nonlinear FE analysis, this subject is mostly treated rather briefly or the focus is on single aspects only.

For reference purposes, the initial focus is on linear static analysis. Subsequently, the various aspects of loading in nonlinear problems as raised above are discussed separately. The discussion particularly focuses on their physical reality

or origin, their different dependencies on deformation, and the resulting consequences for analyses. Finally, it is suggested how a physically reasonable control of loading may be performed. A further interest is on avoiding incomplete models or incorrect boundary conditions. The particular interaction of structures with gas and/or fluid media resulting in pressure often also referred to as follower forces allows an analytical description This topic is discussed in detail including its applications.

The topic of load control–in a standard analysis performed with a single factor–requires specific attention to the high nonlinearities and possible indefinite or negative definite Hessian matrices in the solution process.

In summary, loading is nothing else than one component of our mathematical and mechanical model of physical reality with underlying assumptions and more or less clear limits, which may lead to false conclusions in the worst case.

2 | LOAD MODELING–LOADING IN LINEAR STATIC ANALYSIS

Although this topic is covered in many introductory mechanics textbooks, we will provide a brief overview as it will be referenced later in the discussion of nonlinear cases.

Assuming that we have a structural model in solid mechanics the first considered loading of such a model is caused by masses on which gravitational accelerations–neglecting electrical and magnetic fields also in the following–are acting. The masses are either permanent and thus imply so-called dead loads or masses placed on the structure which underlie gravitation. According to Newton's second law of motion, both masses resp. both types of masses lead to forces on the structure. For the masses placed on the structure Newton's third law of motion for interacting bodies resp. bodies in contact is used in addition. The latter model of interacting bodies can also be applied to any type of media such as fluids and granular media, for example, sand. Both media types are subject to gravitation and, when in contact or interaction with a structure can lead to quite complex load models described by forces and force distributions.

Static loading is also often taken as a simplification of dynamic loading such as inertial forces resulting from earthquake motions or accelerations, or as a replacement for wind loading. Interestingly we also observe quasi-static accelerations in rotating bodies, such as centrifugal forces on rotating masses and structures. Then the models discussed above for gravitation can be applied in the same way.

All the forces described above are usually called external forces thus Neumann boundary conditions in a wider modeling concept in structural mechanics. For the design of structures, well-established procedures such as combining possible loads are available and standard in engineering practice, see engineering standards, for example, Reference 1.

In addition to clearly defined external forces such as gravitational or centrifugal/centripetal forces resulting from masses and accelerations, the following discussion will focus on other loading definitions, mostly resulting from interaction with other bodies or parts of bodies. Using Newton's third law of interacting bodies engineers replace one of the bodies or parts of attached body parts by corresponding loads, see Figure 1. In a more general view of structural mechanics, the other bodies can be solid, beam, or shell-type structures, as well as gaseous, fluid or granular media. As is well known, this very important principle allows to study the parts of the structure separately and, in the case of statically indeterminate structures, to perform the analysis using either the force/flexibility method or the displacement method.

This is a perfect procedure for design, for example, in civil engineering with small deformations, where structural parts are separated into load-bearing parts, while the attached parts are replaced by for example, single-type loads or any kind of distributed loading. If the forces are then increased linearly such a scheme may lead to an oversized design, nevertheless, it is very well suited for the design the major load-carrying parts. A major advantage is that we can make simplifying assumptions and still get a safe structure. A second advantage is the efficiency of defining a main load-carrying structure. Although a more complete analysis of the entire structure–essentially more complex–would take into account the complete stress and strain state, and may reduce inaccuracies and overdesign due to the necessary assumptions, such complex complete models have been less common in civil engineering than in mechanical, automotive, and aerospace engineering.

Todays's available finite element technology in combination with CAD, however, allows detailed three-dimensional and shell-type simulations with a high degree of detail and almost arbitrary nonlinear features concerning large deformations, large displacements, and nonlinear material behavior.

At this point, it is important to distinguish between the external forces or loads and the internal forces and force patterns. If for example, we are interested in the stresses in the granular media, case (D) in Figure 1, then the force pattern acting between the structure and the granular medium must be considered as an internal force pattern, which

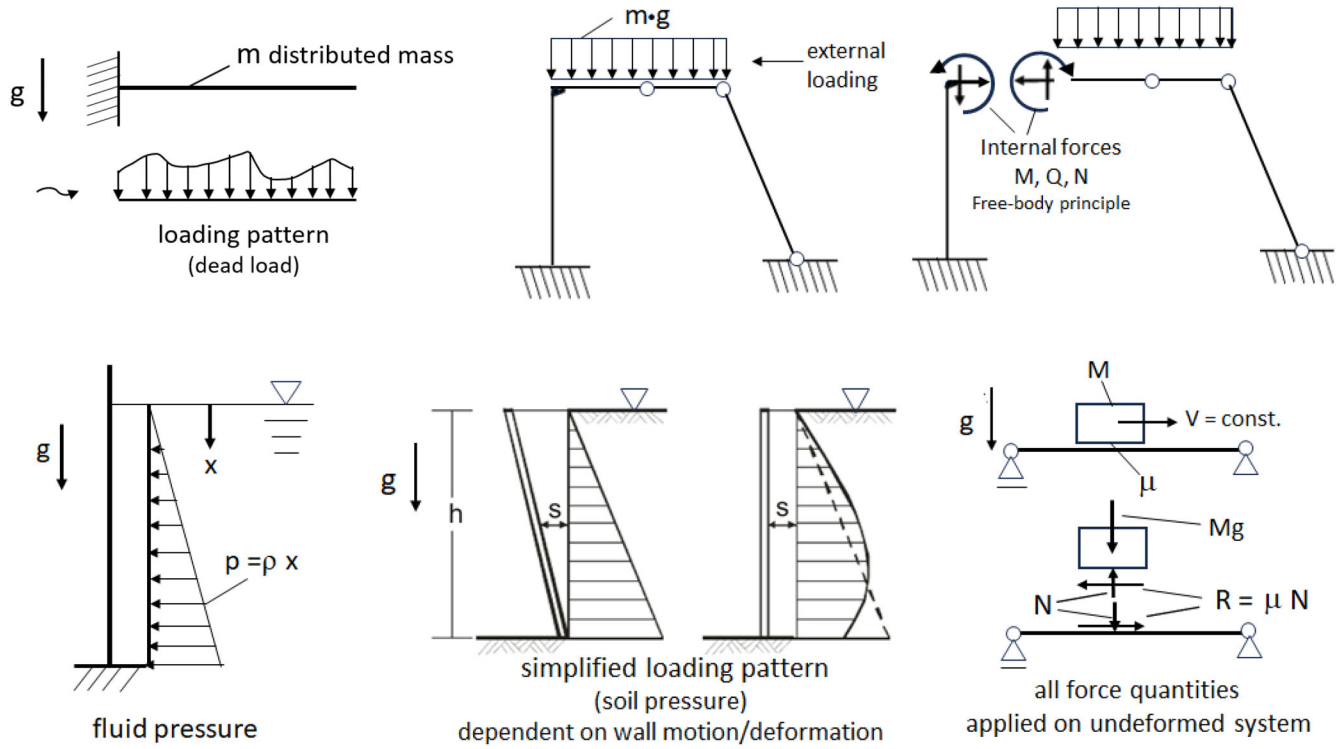

FIGURE 1 Load modeling in linear static analysis as a consequence of gravity. (A) Cantilever beam with nonuniform mass distribution, (B) Beam structure with dead load, (C) Wall under fluid pressure, (D) Walls with soil interaction, (E) Friction with moving mass.

also requires a detailed model for the granular media part, see Figure 1D. This is also the case for fluid and gas loading–considering both as contacting media, see Figure 1C.

However, a closer look reveals a first modeling step of varying complexity for the different loads. Single point loads resulting from single masses or distributed loading/loading patterns due to distributed mass or multiple masses are rather easily defined in the direction of gravity. Any other single load or moment (bending or torsional) loading, or distributed loads or moments are deducted from previous analysis steps as for example, parts within a larger structural model, see Figure 1B. This is also valid for any other type of loading resulting from the various constitutive laws of interaction between contacting bodies for example, static friction or adhesion, see Figure 1E. A previous analysis is also the basis for fluid and gas load models. Both are pressure loads with a known origin, gas within a containment with a prescribed behavior, Poisson's or Boyle's law acting completely uniformly on the walls of the containment, and fluids within a gravity field and a prescribed density showing a linear dependence on the height of the fluid surface acting on a structure, Figure 1C. Thus both are media for which the interaction with structures can be described analytically with geometric and physical laws. In a finite element environment, we often refer to them as meshless models.

As mentioned earlier, load control is achieved fairly simply by increasing the "added" load by a factor–that is, linearly–in order to create a safe design, or by modifying added load patterns, including interactions, to achieve maximum internal forces/stresses. A well proven procedure is also combining traffic loads according to standards[1] and in addition applying safety factors, thus linearly increasing the considered loads and, as a consequence, also the resulting quantities such as stresses.

3 | LOAD MODELING IN NONLINEAR STATIC ANALYSIS

Although modern analysis tools such as finite element methods allow the investigation of complete structures under various loading conditions, the procedures found in linear analysis concerning loading are often transformed and incorporated in reduced models for nonlinear analysis, such as stability investigations and/or large deformation problems for structural components.

3.1 | Distinguishing load models in nonlinear statics

Following Newton's second law of motion we have a simple model of forces acting in or on a structure or solid continuum. A typical example of a more complex problem is the model of the so-called static follower forces, which means that with the deformation of a structure, the loading also changes in a more or less logical way, even defining so-called non-conservative problems, which will be discussed in the following. A simple explanation is given in Figure 2. Deformation dependence can be defined in the following fashion–whether physically possible or not:

a. Single loads
   a1. Point of action changes with deformation, direction of force remains as originally.
   a2. Point of action changes with deformation, direction of loading changes with deformation.
   a3. Magnitude of loading changes with deformation, such as centrifugal force, mass rotating with constant angular velocity.
b. Distributed loading
   b1. Area of action changes, direction of forces remains as originally.
   b2. Area of action changes and direction of loading changes with deformation.
   b3. Magnitude and shape of distributed loading may change with deformation, such as structure under fluid or wind loading, see Figure 3.

For dead loads, the concept is rather simple–such loads, including snow or ice, act in the direction of gravity. However, if the dead loading is due to so-called added masses and traffic loads from bodies positioned or fixed to the structure, careful consideration is needed to determine how much larger deformations will influence their action on the mechanical structure. If we exclude that an added/fixed mass/body is sliding after a deformation which would be a non-stationary process, moment loading results from excentricity such as an attached mass with respect to a reference axis. Therefore,

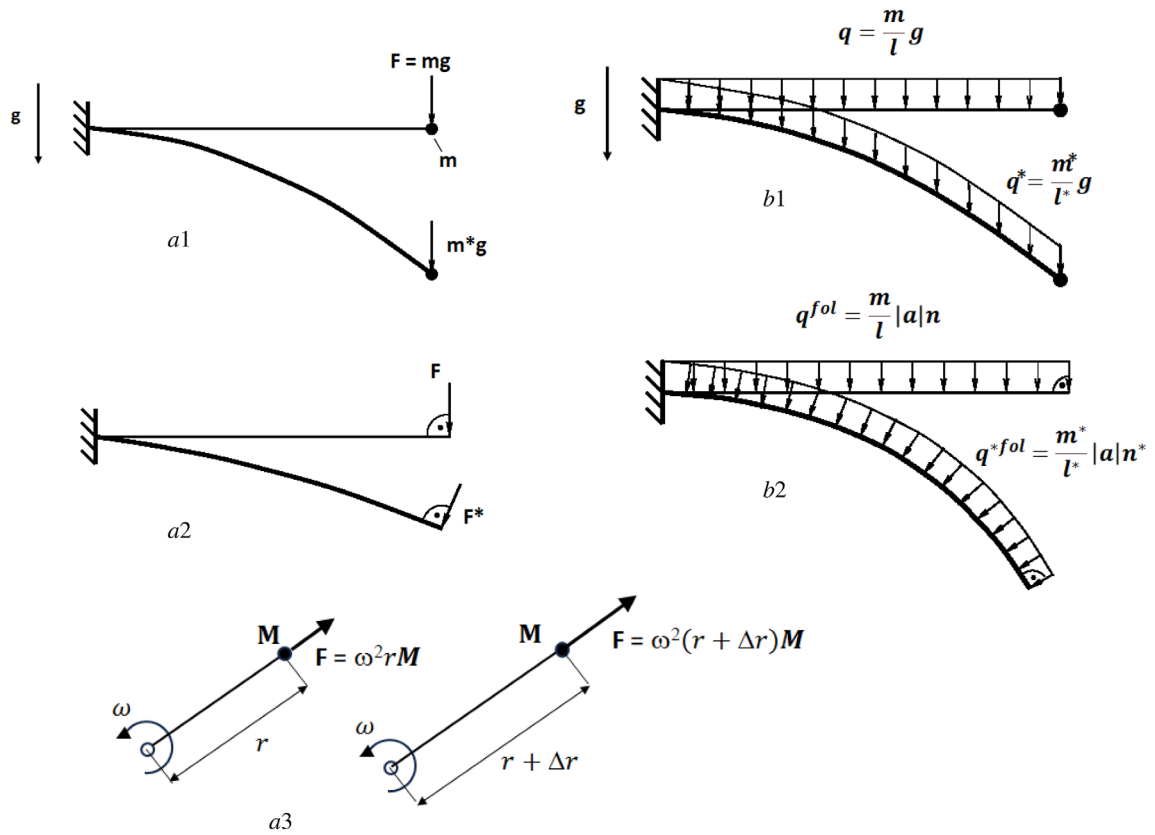

FIGURE 2 Loading cases in nonlinear statics with follower effects for single load and distributed loading. Questionable distributed loading (quasi pressure load) at boundary–See also the discussion in section 4.1.4, Figure 9.

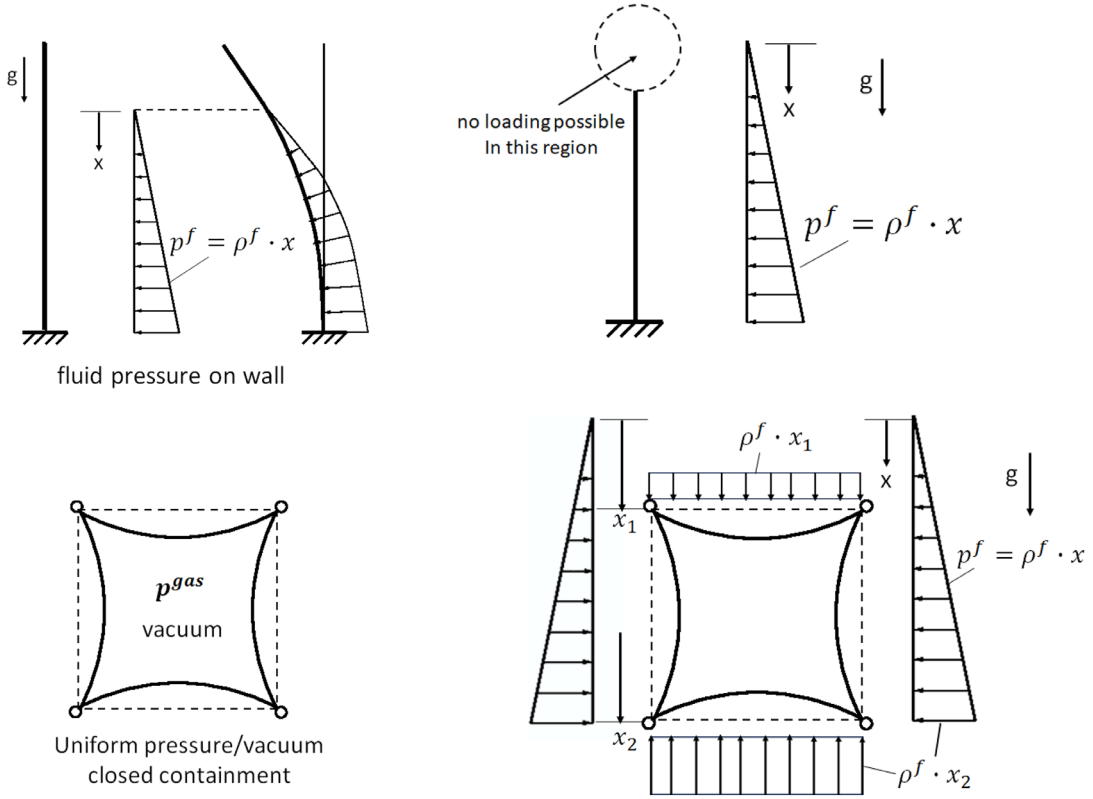

FIGURE 3 Pressure loading by fluids and gas, physically clearly defined cases. Interaction in statics exactly described. Boundary must be considered correctly–No pressure at boundary of structure.

deformation-dependent moments as a separate loading cannot exist without associated forces. Consequently, single and distributed deformation dependent moment loading alone is not possible. Further, in a structure with nonlinear behavior, any internal force computation and thus internal force quantities belong to a certain state and will change continuously with deformation. As a conclusion, we only discuss force loading aspects in the following.

In general, the point of action and the direction of action for single and distributed loads depend on the setup of the structure. Surface loading from dead loading and gravity/accelerations–here added masses or attached masses–acts on parts of the surface or the entire surface.

Pressure loads on surfaces are caused by gas and/or fluid loading, wind loading (using e.g., a maximum loading picture by a stationary load and some factor to incorporate some uncertainty and dynamic effects), and possible interaction with contacting media such as granular solids. In the case of gas and fluids thus hydrostatics, they are acting normal to the surfaces of the considered structures. An important aspect is that pressure loading by gas or fluids is physically restricted–see Figure 3. Gas pressure requires a closed containment also in the simulation model. Fluid loading with open surfaces is possible, but then the fluid surface level must remain below the boundary height. In addition, fluids in closed containments are possible with overpressure and in combination with partial gas and fluid filling.

As previously stated, it is not possible to have pressure at free edges. Therefore, when considering for example, wind loading on non-closed structures as static stationary loading, it is an incomplete model of reality and has limitations for safe design.

The same statements apply to rotating bodies with masses and/or fluids, but in this case, the accelerations are perpendicular to the axis of rotation. For further discussion and references, see section 4.3.1.

3.2 | Discussion of some follower force models

Before describing the mathematical simulation models, we will discuss some aspects of the physical reality of deformation-dependent models.

The first model we will examine is the cantilever beam shown in Figure 2, which is loaded with a single force that always acts perpendicular to the deformed beam axis. It is important to note that no physically realized mechanical device causing such a force has been found in the literature thus far. Even applying a displacement at the tip of the cantilever beam it is impossible to create a reaction force perpendicular to the deformed beam axis without prior knowledge of the axis.

There is a significant amount of literature on force models that act tangentially on a beam axis or plate (mid)surface, often referred to as follower loads or forces. These forces are considered non-conservative as they cannot be derived from a potential. The literature often focuses on the influence of deformation dependence on stability behavior under these forces or force combinations, with specific stability failure occurring through flutter*, and possibly divergence as well. The term "flutter" appears to have originated from the physical and experimental models related to nonconservative forces.

The scientific literature on nonconservative forces see for example, References 2–5 and their effects is accompanied by a very controversial debate about their physical realization in experiments, see for example, Koiter 1996.[6] Koiter even denies completely the existence of such single follower forces. A wide number of models with possible or apparently physical realizations can be found, however, they are mathematical models of the kind of stationary fluid conveying through a thin flexible pipe see for example, Reference 7. It is often unclear whether these models include all the necessary effects to accurately describe the physics. An extensive investigation of mathematical models and their experimental verification can be found in the excellent and comprehensive paper of Elishakoff 2005.[8] It contains painfully clear explanations why all experiments fail to validate the follower-type load models for beams. Careful restrictions are given towards some not well-documented resp. hard to follow experiments. Some interesting physically completely contradictory results of mathematical models are also given accompanied by a very large literature review.

Some forces created for example, from sliding in frictional contact problems, see Figure 4 can also be viewed as follower forces when a stationary friction process is present. However, while the friction force can be maintained in one direction it is certainly hard to guarantee a purely tangential follower force even with some sideward deflection. Nevertheless, in Reference 9 the authors claim to have found a mechanical device using some anisotropic surface structure to create anisotropic friction which allows to observe instability by flutter as well as by divergence and they obtained critical values very close to those computed in one of the first publications[3] on this subject.

As mentioned, all the experiments have some dynamics involved–either by a stationary motion of a conveying fluid or stationary friction, which introduces a specific modeling step into the quasi-static mechanical simulation model. For most at least Newton-type forces the observation of Koiter[6] and the critical review of Elishakoff[8] make these non-conservative forces a questionable model.

Another type of follower force appears to result from the application of the free-body principle. In such models, the internal forces or only part of them are taken as if being external forces and considered then as following the deformation of a structure. Typical examples are some widely used loadings in the finite element literature, see Figure 5.

The roll-up of a beam due to moment loading is an often taken example to show the capacity of FE developments. Interestingly this loading case has already been worked on by Euler 1744 see Reference 10 with an analytical solution. The excuse for using such physically non-existent loading possibly also created from stress patterns nowadays is their application for scientific (academic) reasons only for example, for testing some newly developed finite elements and algorithms with very large deformations. The same argument may be valid, if bending and or torsional moments usually gained from the free-body principle are applied, which are definitely no external resp. Newton-type force quantities.

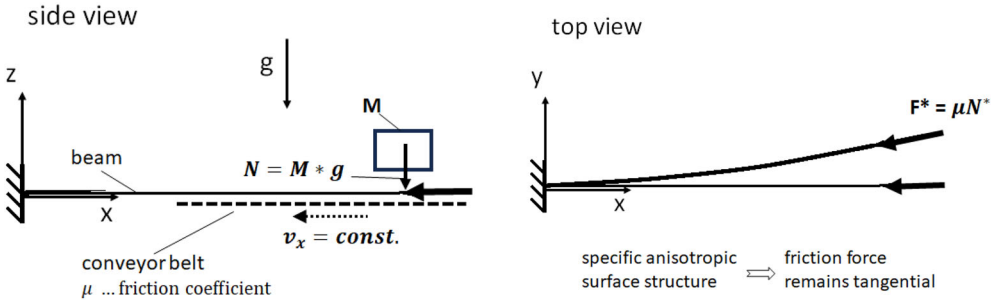

FIGURE 4 Follower force loading created by a stationary friction force. Mechanism after Reference 9.

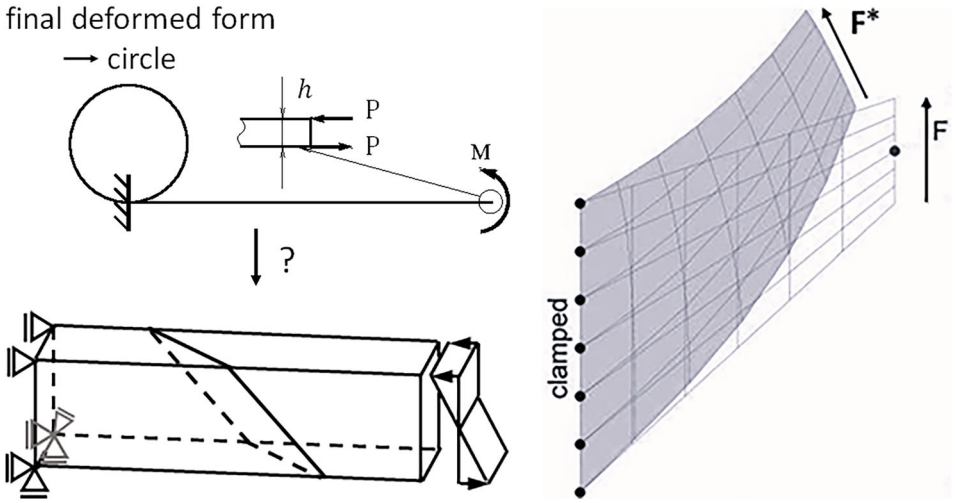

FIGURE 5 Questionable deformation dependent/follower force loading–classical roll-up of a flexible beam–found in scientific Finite Element applications. Pure moment and pure shear loading.

4 | REALISTIC MODELING OF GAS-FLUID-STRUCTURE INTERACTION AND LITERATURE REVIEW

We restrict now our view purely to fluid and gas interaction–directly described via geometry and by physical laws–with structures in quasi-static states. Such constellations occur in underwater structures or submarines and all kinds of enclosed volumes such as tires, airbags or balloons. However, it should be noted that in the engineering design of such lightweight structures prone to instability the loss of stability is not allowed by design for example, for tires and for submarines especially for bathyscaphes. Then besides the direction dependence of the loading and the area change of the loaded parts due to deformation, the volume change within the loading process has often a major effect on the local pressure. The latter is of greater interest if pneumatic structures are taken to achieve a local closure for structural parts for example, gas lines or as air inflated and/or fluid filled dams, see section 6.

The applications in practice show, how important it is to have complete control over the pressure loading and its effects on the surrounding structures. Interestingly, in industrial practice volume effects have been mainly taken into account in airbag and hydroforming analysis with so-called explicit FE programs such as for example, Reference 11. There only dynamic resp. quasi-static processes taking the inertia of the structures into account can be simulated, however with very small time steps. Due to the nature of the time integration algorithm–central differences–no information is directly available about for example, stability, as no tangent matrices are set up.

Within the following, our focus is on the derivations for static resp. implicit solution schemes to allow stability and large deformation FE analyses.

4.1 | Formal treatment of distributed forces with large deformations–Gas-/fluid-structure interaction

Besides the direct physical argumentation given above, we will show exemplarily the consistent development of gas and fluid interaction with structures–well known as deformation dependent loading- using a standard procedure in finite element technology. Looking into the literature, deformation dependence for stability type problems with small deformations–the stability load of long cylinders under external pressure is then reduced by a quarter compared to neglecting this effect–is known since long.[12] Further more general theoretical developments exist already some time ago, see References 13,14 giving insight into the nature of so-called configuration dependent loading and conservative systems.

Assuming the description of the general nonlinear structural behavior in a standard fashion via the virtual work principle our focus is only on the gas- and fluid-interaction thus the external virtual work of a pressure load for the structure part and on the additional equations specifying the physical behavior of the gas and the fluid. The following derivations are based on developments described in our first works for nonlinear statics and stability see References 15,16.

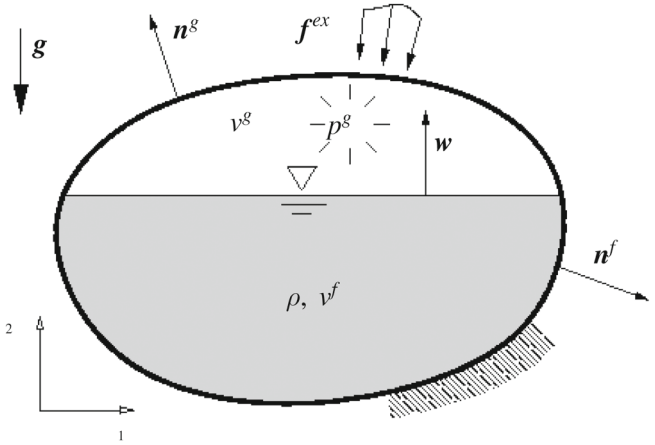

FIGURE 6 Shell structure filled with fluid and gas.

For further work we refer for axisymmetric problems to Reference 17, for a pneumatic element to Reference 18, for air supported membranes to Reference 19, for partially fluid and gas filled containers to Reference 20, and to extensions from our group see References 21,22. A general formulation involving all possible cases of multi-chambers with partial fluid and gas filling is given in References 23 and 24.

Here we restrict us to the fairly general case of a single structure–a closed flexible container filled with fluid and gas and loaded by an external load $\boldsymbol{f}^{ex}$–of course, as discussed above, created by a mass and gravity acceleration or by a body in contact, see Figure 6. Within the framework of virtual work, we focus on the terms associated to fluid and gas. Assuming a current state with a gas volume v^g and a gas pressure p^g, a fluid volume v^f, gravity g, a fluid pressure p^f, the pressure on the structure is clearly dependent on the current position $\mathbf{x}$ of all surface points of the structure, the normal of the surface $\mathbf{n}^*$ the total virtual work expression can be written as:

$$\delta\Pi = \delta\Pi^{el} + \delta\Pi^{press} - \delta W^{ex} = 0 \tag{1}$$

Thus the virtual work of the actual state is given by the structural part $\delta\Pi^{el}$–for simplicity elastic, the work of the external loading δW^{ex} and the virtual work of the pressure resulting from gas $\delta\Pi^g$ and from fluid $\delta\Pi^f$. In the following, the focus is only on the virtual work of the fluid-structure-interaction part thus the gas and fluid loading. The pressure level p is then dependent on the current position $\mathbf{x}$ of all surface points of the structure in space and their current position relative to the free fluid surface and for the gas part dependent on the current gas volume $v^g(\mathbf{x})$. The fluid contacting part is described with the index f and the gas contacting part with g. The external virtual work of the pressure terms becomes:

$$\delta\Pi^{press} = \int_a p\ \mathbf{n}^* \cdot \delta\mathbf{u}\ da \tag{2}$$

with the general normal definition $\mathbf{n}^* = \frac{\mathbf{x}_{,\xi}\times\mathbf{x}_{,\eta}}{|\mathbf{x}_{,\xi}\times\mathbf{x}_{,\eta}|}$, the virtual displacement $\delta\mathbf{u}$, the general surface element $da = |\mathbf{x}_{,\xi} \times \mathbf{x}_{,\eta}|\ d\xi d\eta$ of the surfaces contacted by fluid or gas a^f and a^g and the pressure level p^f resp. p^g. The position vector $\mathbf{x}(\xi,\eta)$ depends on local coordinates ξ, η. Thus the pressure is acting perpendicular to the surface of the structure; the surface da may be modified under loading in size, the latter represented by $|\mathbf{x}_{,\xi}\times\mathbf{x}_{,\eta}|$. Multiplying $\mathbf{n}^*\ da$ a non-normalized form $\mathbf{n} = \mathbf{x}_{,\xi}\times\mathbf{x}_{,\eta}$ of the normal vector $\mathbf{n}^*$ is introduced, resulting in gas and fluid surface parts:

$$\delta\Pi_{press} = \int_\eta\int_\xi p\ \mathbf{n}\cdot\delta\mathbf{u}\ d\xi d\eta = \int_{\eta^f}\int_{\xi^f} p^f\ \mathbf{n}^f\cdot\delta\mathbf{u}^f\ d\xi d\eta + \int_{\eta^g}\int_{\xi^g} p^g\ \mathbf{n}^g\cdot\delta\mathbf{u}^g\ d\xi d\eta. \tag{3}$$

The physical behavior of the gas is specified by Poisson's law resp. an adiabatic change; κ as isentropy constant, P, V as initial pressure resp. volume for the gas volume:

$$p_t\ v_t^\kappa = P\ V^\kappa = const. \tag{4}$$

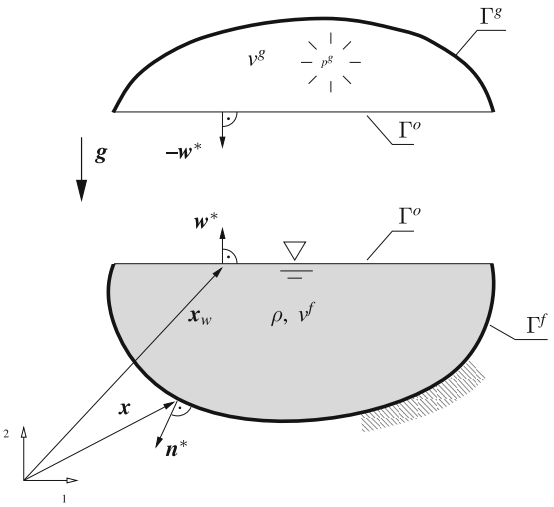

FIGURE 7 Sectioning of control volumes v^g and v^f.

The interesting aspect is the computation of the actual volume of the gas part. It is assumed that the volume v^g is described by its corresponding surface and is computed via:

$$v^g = \frac{1}{3}\int_\eta\int_\xi \mathbf{x}^g \cdot \mathbf{n}^g \; d\xi d\eta. \tag{5}$$

Virtual work of fluid volume compression could be added, however, in the following only the case of heavy incompressible fluids is presented. Thus the fluid volume is kept constant, for compressible fluids see Reference 22.

The pressure distribution in the fluid filled part is described by the hydrostatic pressure law (6)–here without the gas pressure at the fluid surface–and the volume conservation condition Equation (7) of the contained fluid–assuming incompressibility.

$$p^f = \gamma_i(\mathbf{x}_w - \mathbf{x}) \cdot \mathbf{w} \tag{6}$$

$$v^f = const. \tag{7}$$

With $\gamma_i = \rho\, g$ as specific gravity, ρ as specific density of the fluid, g as the acceleration due to gravity, $\mathbf{x}_w$ as position vector to the fluid surface and $\mathbf{w}^*$ as unit normal vector on the fluid surface, see Figure 7. The volume v^f of the fluid can then be computed via:

$$v^f = \frac{1}{3}\int_\eta\int_\xi (\mathbf{x}\cdot\mathbf{n} + \mathbf{x}_w \cdot \mathbf{w}) \; d\xi d\eta. \tag{8}$$

Corresponding to the non-normalized normal vector $\mathbf{n}$ on the submerged surface of the structure, $\mathbf{w} = \mathbf{x}_{wi,\xi} \times \mathbf{x}_{wi,\eta}$ denotes the non-normalized normal vector of the free fluid surface. It must be noted that $\mathbf{w}$ has the identical direction as $-\mathbf{g}$ for any fluid surface due to gravity.

Thus the major difference to a closed volume with either only gas or only fluid–for the latter then compressibility would be needed–is simply the fact that together with the submerged surface of the structure the fluid surface describes the closure of the considered fluid volume part.

4.1.1 | Linearization of the virtual work expression of the pressure terms

Considering the computational model for finite element simulations with shell, volume, or beam element surfaces and assuming nonlinear behavior, the system of nonlinear equations resulting from the variational expression must be linearized for the solution with a Newton-type scheme. Then the linearization at state t has to be performed before the

discretization with for example, Finite Elements and within an incremental iterative procedure. In the following, we restrict us to both pressure terms, gas, and fluid. The necessary quantities are X as initial position of a structural surface point, $\mathbf{x}_t = \mathbf{X} + \mathbf{u}_t$ as known position at state t, and therefore $\mathbf{x} = \mathbf{x}_t + \Delta\mathbf{u}$ as position at the current state of the structure. The different contributions have to be linearized separately. Hereby $P(\mathbf{X}_w, \mathbf{X})$, V denote the initial pressure and volume, $p_t = p_t(\mathbf{x}_w, \mathbf{x})$, v_t are the known pressure and volume respectively following Equation (4). The expression for the external virtual work of the considered volume includes the linear part of the changes of the normal and of the pressure change. Both are integrated over the correspondingly submerged surface:

$$\delta\Pi^{lin}_{press} = \delta\Pi_{press,t} + \delta\Pi^{\Delta p}_{press,t} + \delta\Pi^{\Delta \mathbf{n}}_{press,t} \tag{9}$$

$$\delta\Pi^{lin}_{press} = \int_\eta \int_\xi (p_t\ \mathbf{n}_t \cdot \delta\mathbf{u} + \Delta p\ \mathbf{n}_t \cdot \delta\mathbf{u} + p_t\ \Delta\mathbf{n} \cdot \delta\mathbf{u})\ d\xi d\eta \tag{10}$$

$$\text{with} \quad \Delta\mathbf{n} = \Delta\mathbf{u}_{,\xi} \times \mathbf{x}_{t,\eta} - \Delta\mathbf{u}_{,\eta} \times \mathbf{x}_{t,\xi} \tag{11}$$

for the change of the non-normalized linearized normal vector. Equation (11) represents the Taylor expansion up to linear terms.

4.1.2 | Linearization of Poisson's law, the gas volume, the hydrostatic pressure law and the volume conservation condition for the fluid

As the gas law indicates that the product of its components remains constant, the change of the product is zero:

$$\Delta(pv^\kappa) = 0 \qquad \text{thus} \qquad \Delta p\ v_t^\kappa + \qquad \Delta v^\kappa\ p_t = 0 \tag{12}$$

$$\text{whereby} \quad \Delta v^\kappa = \kappa \frac{v_t^\kappa}{v_t} \Delta v^g. \tag{13}$$

Finally the linearized expression for the adiabatic change results in:

$$\Delta p^g + \frac{\kappa p_t^g}{v_t^g} \Delta v^g = 0 \qquad \text{with} \qquad \Delta v^g = \frac{1}{3} \int_\eta \int_\xi (\Delta\mathbf{u} \cdot \mathbf{n}_t + \mathbf{x}_t \cdot \Delta\mathbf{n})\ d\xi d\eta \ \equiv\ \Delta v^g_{\Delta\mathbf{u}} + \Delta v^g_{\Delta\mathbf{n}}. \tag{14}$$

The linearized hydrostatic pressure and the volume conservation condition can be written for the fluid part as:

$$\Delta p^f = \gamma(\Delta\mathbf{u}_w - \Delta\mathbf{u}) \cdot \mathbf{w} \tag{15}$$

$$\Delta v^f = \frac{1}{3} \int_\eta \int_\xi (\Delta\mathbf{u} \cdot \mathbf{n}_t + \mathbf{x}_t \cdot \Delta\mathbf{n} + \Delta\mathbf{u}_w \cdot \mathbf{w}_t + \mathbf{x}_{w,t} \cdot \Delta\mathbf{w})\ d\xi d\eta = 0 \tag{16}$$

$$\equiv \Delta v^f_{\Delta\mathbf{u}} + \Delta v^f_{\Delta\mathbf{n}} + \Delta v^f_{\Delta\mathbf{u}_w} + \Delta v^f_{\Delta\mathbf{w}} = 0. \tag{17}$$

Where $\mathbf{x}_w = \mathbf{x}_{w,t} + \Delta\mathbf{u}_w$ is the current fluid level, and $\Delta\mathbf{w}$ is the change of the non-normalized normal vector of the free fluid surface, see Figure 7. The volume change Δv^f–in total zero–can be expressed as shown in Equations (16) and (17) by the volume change due to the displacements of the structure $\Delta v^f_{\Delta\mathbf{u}}$, the fluid level $\Delta v^f_{\Delta\mathbf{u}_w}$, the volume change due to the change of the normals on the submerged structure $\Delta v^f_{\Delta\mathbf{n}}$ and the free fluid surface $\Delta v^f_{\Delta\mathbf{w}}$.

4.1.3 | Complete virtual work of gas and fluid–Reformulation for finite element discretization

Now using the equations above the complete virtual work expressions and the linearized expressions for the combined gas and fluid loading in a containment can be written for use e.g. in a Newton-type solution procedure at a given state $t^\dagger$.

- *Residual*

$$\delta\Pi^{f+g}_{lin} = \int_{\eta^f} \int_{\xi^f} p_t^f \boldsymbol{n}_t^f \cdot \delta\boldsymbol{u}^f\ d\xi d\eta + \int_{\eta^g} \int_{\xi^g} p_t^g \boldsymbol{n}_t^g \cdot \delta\boldsymbol{u}^g\ d\xi d\eta \tag{18}$$

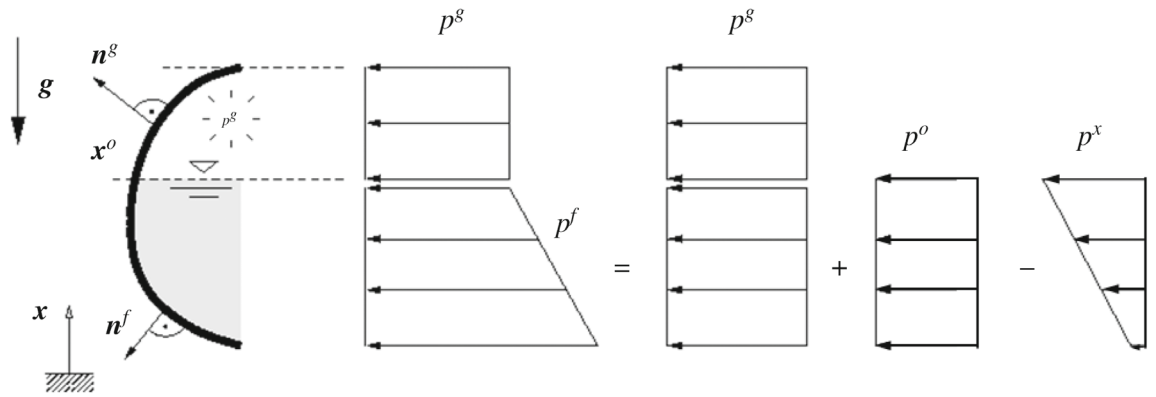

FIGURE 8 Hydrostatic pressure distribution in a containment filled with gas and incompressible heavy fluid.

- *Pressure change parts*

$$+\int_{\eta^f}\int_{\xi^f}\Delta p^f \boldsymbol{n}_t^f\cdot\delta\boldsymbol{u}^f\,d\xi d\eta+\int_{\eta^g}\int_{\xi^g}\Delta p^g\boldsymbol{n}_t^g\cdot\delta\boldsymbol{u}^g\,d\xi d\eta \tag{19}$$

- *Normal change parts*

$$+\int_{\eta^f}\int_{\xi^f}p_t^f\Delta\boldsymbol{n}^f\cdot\delta\boldsymbol{u}^f\,d\xi d\eta+\int_{\eta^g}\int_{\xi^g}p_t^g\Delta\boldsymbol{n}^g\cdot\delta\boldsymbol{u}^g\,d\xi d\eta. \tag{20}$$

The hydrostatic pressure distribution is depicted in Figure 8, defining the terms for p^f in this specific case. As a special case, the filling with gas only is included. In the case of a containment fully filled with fluid, the compressibility of the fluid has to be taken into account, see Reference 23. Thus the fluid pressure part p^f is composed of three parts: the general linear displacement part p^x, the constant part p^0 dependent on the fluid level $\boldsymbol{x}^o$ and the gas pressure p^g:

$$p^x=\rho^f\boldsymbol{g}\cdot\boldsymbol{x},\qquad p^o=\rho^f\boldsymbol{g}\cdot\boldsymbol{x}^o,\qquad \text{thus}\qquad p^f=p^g+p^o-p^x. \tag{21}$$

4.1.4 | Partial integration–Check of conservativeness

For using the virtual expression and the linearized version in a finite element context partial integration helps to get proper information on the structure of the corresponding load vector, stiffness matrices, and boundary conditions. For this rather lengthy process we refer to own contributions[21,22,25] and a complete summary of all possible combinations of gas and compressible as well as incompressible fluid in multiple chambers and external loading given by References 23,24. The final result is split into two parts, a term mainly based on the change of the normal and a second term dominantly based on the pressure change. Important for the derived form is the partial transformation to a contravariant basis.

Normal change part: Introducing thus skewsymmetric tensors $\boldsymbol{w}$ in a convective basis $\boldsymbol{x}^{,\bar{\xi}}\otimes\boldsymbol{x}^{,\bar{\eta}}$, with $\bar{\xi}$, $\bar{\eta}$ as the contravariant curvilinear coordinates,

$$\boldsymbol{W}^{\bar{\xi}}=\boldsymbol{n}_t\otimes\boldsymbol{x}^{,\bar{\xi}}-\boldsymbol{x}^{,\bar{\xi}}\otimes\boldsymbol{n}_t \tag{22}$$

$$\boldsymbol{W}^{\bar{\eta}}=\boldsymbol{n}_t\otimes\boldsymbol{x}^{,\bar{\eta}}-\boldsymbol{x}^{,\bar{\eta}}\otimes\boldsymbol{n}_t \tag{23}$$

we obtain the normal change parts as follows for both, gas and fluid domains:

$$\delta\Pi_{lin}^{\Delta n^g}=\int_{\eta^g}\int_{\xi^g}\frac{p_t^g}{2}\begin{pmatrix}\delta\boldsymbol{u}^g\\ \delta\boldsymbol{u}^g_{,\xi}\\ \delta\boldsymbol{u}^g_{,\eta}\end{pmatrix}\cdot\begin{pmatrix}\boldsymbol{0}&\boldsymbol{W}^{\bar{\xi}}&\boldsymbol{W}^{\bar{\eta}}\\ \boldsymbol{W}^{\bar{\xi}T}&\boldsymbol{0}&\boldsymbol{0}\\ \boldsymbol{W}^{\bar{\eta}T}&\boldsymbol{0}&\boldsymbol{0}\end{pmatrix}\begin{pmatrix}\Delta\boldsymbol{u}^g\\ \Delta\boldsymbol{u}^g_{,\xi}\\ \Delta\boldsymbol{u}^g_{,\eta}\end{pmatrix}d\xi d\eta \tag{24}$$

$$\delta\Pi_{lin}^{\Delta n^f} = \int_{\eta^f}\int_{\xi^f} \frac{p_t^f}{2} \begin{pmatrix} \delta \boldsymbol{u}^f \\ \delta \boldsymbol{u}^f_{,\xi} \\ \delta \boldsymbol{u}^f_{,\eta} \end{pmatrix} \cdot \begin{pmatrix} \mathbf{0} & \boldsymbol{W}^{\bar{\xi}} & \boldsymbol{W}^{\bar{\eta}} \\ \boldsymbol{W}^{\bar{\xi}T} & \mathbf{0} & \mathbf{0} \\ \boldsymbol{W}^{\bar{\eta}T} & \mathbf{0} & \mathbf{0} \end{pmatrix} \begin{pmatrix} \Delta \boldsymbol{u}^f \\ \Delta \boldsymbol{u}^f_{,\xi} \\ \Delta \boldsymbol{u}^f_{,\eta} \end{pmatrix} d\xi d\eta$$
$$- \frac{\rho^f}{2} \int_{\eta^f}\int_{\xi^f} \delta \boldsymbol{u}^f \left(\boldsymbol{n}_t^f \otimes \boldsymbol{g} - \boldsymbol{g} \otimes \boldsymbol{n}_t^f \right) \cdot \Delta \boldsymbol{u}^f \; d\xi d\eta \tag{25}$$

From the **pressure changes** we obtain the following parts:

$$\begin{aligned} \delta\Pi_{lin}^{f+g} = (\alpha_t - \gamma_t) & \int_{\eta^f}\int_{\xi^f} \boldsymbol{n}_t^f \cdot \delta \boldsymbol{u}^f \; d\xi d\eta \int_{\eta^f}\int_{\xi^f} \boldsymbol{n}_t^f \cdot \Delta \boldsymbol{u}^f \; d\xi d\eta \\ + \alpha_t & \int_{\eta^f}\int_{\xi^f} \boldsymbol{n}_t^f \cdot \delta \boldsymbol{u}^f \; d\xi d\eta \int_{\eta^g}\int_{\xi^g} \boldsymbol{n}_t^g \cdot \Delta \boldsymbol{u}^g \; d\xi d\eta \\ + \alpha_t & \int_{\eta^g}\int_{\xi^g} \boldsymbol{n}_t^g \cdot \delta \boldsymbol{u}^g \; d\xi d\eta \int_{\eta^f}\int_{\xi^f} \boldsymbol{n}_t^f \cdot \Delta \boldsymbol{u}^f \; d\xi d\eta \\ + \alpha_t & \int_{\eta^g}\int_{\xi^g} \boldsymbol{n}_t^g \cdot \delta \boldsymbol{u}^g \; d\xi d\eta \int_{\eta^g}\int_{\xi^g} \boldsymbol{n}_t^g \cdot \Delta \boldsymbol{u}^g \; d\xi d\eta \end{aligned} \tag{26}$$

$$\text{with} \quad \alpha_t = \kappa \frac{p^g}{v^g} \quad \text{and} \quad \gamma_t = -\rho^f \left(\int_{\eta^f}\int_{\xi^f} \boldsymbol{n}_t^f \cdot \boldsymbol{g} d\xi d\eta \right)^{-1} \tag{27}$$

In addition to the above domain terms, the subsequent application of the Gauss theorem leads also to boundary terms of the following form using for illustration purposes a Cartesian coordinate system at the boundary s. Then the normal vector $\mathbf{n}_t^s$ and the tangent vector $\mathbf{t}_t^s$ can be written with n_ξ^s, n_η^s as coordinates of the covariant system as:

$$\begin{pmatrix} \mathbf{n}_t^s \\ \mathbf{t}_t^s \end{pmatrix} = \begin{bmatrix} n_\xi^s & n_\eta^s \\ -n_\eta^s & n_\xi^s \end{bmatrix} \begin{pmatrix} \mathbf{g}_\xi \\ \mathbf{g}_\eta \end{pmatrix}. \tag{28}$$

The boundary term of the external virtual work becomes then:

$$\delta\Pi_{press,t}^{\Delta \mathbf{n},boun} = \int_s p_t^s (\Delta \mathbf{u}^s \times \mathbf{t}_t^s) \cdot \delta \mathbf{u}^s \; ds. \tag{29}$$

The boundary integral vanishes, if one of the following five conditions is valid, see also Figure 9.

- **C1** Fixed boundary: $\Delta \mathbf{u}^s = 0$
- **C2** No loading p on complete boundary s: $p_t^s = 0$. This is valid for the surface boundary of structures that are not completely filled with fluid.
- **C3** For any boundary with $p \neq 0$, p.e. pressurized gas on the top of the fluid.
  a) Only displacements parallel to the considered boundary s are allowed: $\Delta \mathbf{u}^s \| \mathbf{t}_t^s \rightarrow \Delta \mathbf{u}^s \times \mathbf{t}_t^s = \mathbf{0}$. This is physically clear as $\mathbf{t}_t^s$ is perpendicular to $p_t^s \mathbf{n}_t^s$ and the virtual work expression vanishes.
  b) One boundary displacement component perpendicular to the tangent vector is fixed: $(\Delta \mathbf{u}^s \times \mathbf{t}_t^s) \cdot \delta \mathbf{u}^s = 0$. Typical for sliding boundary conditions.
- **C4** There is no boundary, thus only closed structures completely filled with gas or fluid are considered as is the case considered above.
- **C5** The boundary integral vanishes as a whole, which is hard to interpret physically.

As a summary–looking at the above-derived forms for the linearized virtual work of fluid and gas pressure–the expressions are symmetric if the physically correct boundary conditions are present. This is clear proof of conservativeness, see References 12–14 for uniform pressure and References 26–29 for hydrostatics, see also Reference 30 for the above-considered problem and those which can be directly taken from the above equations, such as structures completely filled with gas or surrounded by gas pressure, or structures filled with gas and completely surrounded by fluid–underwater structures and similar. For general problems involving gas, fluid, and multiple containments in arbitrary configurations

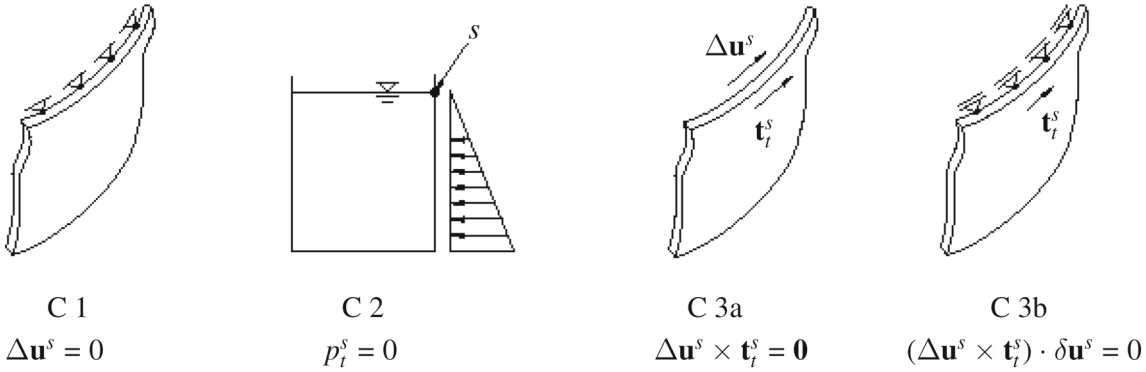

FIGURE 9 Boundary conditions leading to the disappearance of the boundary integral.

see Reference 23. At this point we have to mention that already[31] points out for uniform pressure and two-dimensional problems that the occurrence of nonsymmetric terms is due to the boundary conditions and for closed systems the load stiffness matrix is symmetric.

As conclusion in general we can note that any physically permissible–fitting the boundary conditions in Figure 9–structural problem involving any type of fluid and gas pressure loading can be viewed as being conservatively loaded. As a consequence on the other side, any other distributed loading type must be proved to be physically permissible that is, must be realized constructively. This confirms finally the arguments in section 3.

4.2 | Finite element discretization

After discretizing the linearized virtual fluid structure interaction expression with isoparametric shape functions forming the discretization matrix $\boldsymbol{N}$ for the displacements, the virtual displacements and the incremental displacements of the structural parts that are in contact with gas/fluid in the state t take the following form

$$\boldsymbol{u} = \boldsymbol{N}\boldsymbol{d}\,, \qquad \delta\boldsymbol{u} = \boldsymbol{N}\delta\boldsymbol{d}, \tag{30}$$

we obtain from the normal change parts of Equations (24) and (25) the symmetric load stiffness matrices for each structural element in contact with gas and/or fluid (see also References 15,21,22,25,32):

$$\boldsymbol{K}^g_{elem} = \frac{1}{2}\int_{\eta^g}\int_{\xi^g} p_t^g \begin{pmatrix} \boldsymbol{N} \\ \boldsymbol{N}_{,\xi} \\ \boldsymbol{N}_{,\eta} \end{pmatrix}^T \begin{pmatrix} \boldsymbol{0} & \boldsymbol{W}^{\overline{\xi}} & \boldsymbol{W}^{\overline{\eta}} \\ \boldsymbol{W}^{\overline{\xi}T} & \boldsymbol{0} & \boldsymbol{0} \\ \boldsymbol{W}^{\overline{\eta}T} & \boldsymbol{0} & \boldsymbol{0} \end{pmatrix} \begin{pmatrix} \boldsymbol{N} \\ \boldsymbol{N}_{,\xi} \\ \boldsymbol{N}_{,\eta} \end{pmatrix} d\xi d\eta\,, \tag{31}$$

$$\begin{aligned} \boldsymbol{K}^f_{elem} = \frac{1}{2}\int_{\eta^f}\int_{\xi^f} p_t^f \begin{pmatrix} \boldsymbol{N} \\ \boldsymbol{N}_{,\xi} \\ \boldsymbol{N}_{,\eta} \end{pmatrix}^T \begin{pmatrix} \boldsymbol{0} & \boldsymbol{W}^{\overline{\xi}} & \boldsymbol{W}^{\overline{\eta}} \\ \boldsymbol{W}^{\overline{\xi}T} & \boldsymbol{0} & \boldsymbol{0} \\ \boldsymbol{W}^{\overline{\eta}T} & \boldsymbol{0} & \boldsymbol{0} \end{pmatrix} \begin{pmatrix} \boldsymbol{N} \\ \boldsymbol{N}_{,\xi} \\ \boldsymbol{N}_{,\eta} \end{pmatrix} d\xi d\eta \\ - \frac{\rho_t}{2}\int_{\eta^f}\int_{\xi^f} \boldsymbol{N}^T\left(\boldsymbol{n}_t^f \otimes \boldsymbol{g} + \boldsymbol{g} \otimes \boldsymbol{n}_t^f\right)\boldsymbol{N}\, d\xi d\eta\,. \end{aligned} \tag{32}$$

The residual for the corresponding element results in negative right-hand side vectors due to fluid and gas pressure loading/support is:

$$\boldsymbol{f}^g_{elem} = -\int_{\eta^g}\int_{\xi^g} p_t^g \boldsymbol{N}^T \boldsymbol{n}_t^g\, d\xi d\eta, \tag{33}$$

$$\boldsymbol{f}^f_{elem} = \int_{\eta^f}\int_{\xi^f} (-p_t^g + p_t^o - p_t^x)\boldsymbol{N}^T \boldsymbol{n}_t^f\, d\xi d\eta. \tag{34}$$

Hence along with the coupling vectors reflecting the closed volumes

$$\boldsymbol{a}_{elem} = \int_{\eta^g} \int_{\xi^g} \boldsymbol{N}^T \boldsymbol{n}_t^g \, d\xi d\eta \quad \text{and} \tag{35}$$

$$\boldsymbol{b}_{elem} = \int_{\eta^f} \int_{\xi^f} \boldsymbol{N}^T \boldsymbol{n}_t^f \, d\xi d\eta \tag{36}$$

for the elements in contact with gas/fluid and after assembling all local arrays in their corresponding global arrays the linearized state of equilibrium for a closed system partially filled with an incompressible fluid and gas can be written as:

$$\left(\boldsymbol{K}^{struct} + \boldsymbol{K}^g + \boldsymbol{K}^f + \alpha_t(\boldsymbol{a}+\boldsymbol{b})(\boldsymbol{a}+\boldsymbol{b})^T - \gamma_t \boldsymbol{b}\boldsymbol{b}^T\right)\Delta\boldsymbol{d} = \boldsymbol{f}^{ex} - \boldsymbol{f}^{struct} - \boldsymbol{f}^f - \boldsymbol{f}^g. \tag{37}$$

In Equation (37) the volume dependence of the enclosed gas and fluid is reflected in the rank updates of the stiffness matrix with two symmetric dyadic products of the coupling vectors for each closed volume besides the corresponding residual terms. For both cases gas only–$\rho_t = 0$–or fluid only–$p^g = 0$–each leads to a single dyadic product, thus a symmetric rank-one update of the stiffness matrix.

The load stiffness matrices $\boldsymbol{K}^g$ and $\boldsymbol{K}^f$ have the same bandwidth as the structural stiffness matrix $\boldsymbol{K}^{struct}$ as they are computed via integrals over the submerged surfaces. A standard integration scheme can be used as the fluid pressure is only linearly dependent on the geometry for the stiffness terms as well as for the force terms. For positions beyond the fluid surface, the pressure is constant or null in the case of no gas. The question is, how to capture the pressure of the fluid close to the fluid surface. Our numerical procedure did not apply a specific integration scheme in the vicinity of the fluid surface, as the pressure due to the fluid terms is then anyhow rather small within a reasonably fine mesh of the finite element model. In addition, the finite element interpolation also disperses this effect, unless the fluid level is located exactly on the boundary of the elements. However, some more recent contributions have a specific focus on capturing this region more accurately, see References 33 and 34 both with the general fluid-structure formulation as in References 21,22,35. If the more accurate fluid level computation leads to somehow more accurate results in deformations or stresses remains to be discussed.

The rank updates $\alpha_t(\boldsymbol{a}+\boldsymbol{b})(\boldsymbol{a}+\boldsymbol{b})^T$ and $\gamma_t \boldsymbol{b}\boldsymbol{b}^T$ are linking all variables together leading to a full stiffness matrix for the variables of the submerged finite elements. Thus specific measures have to be taken within the global solution scheme to achieve an efficient algorithm.

A further interesting observation is that in the literature the element load stiffness matrices–not derived via the above-shown process–are often unsymmetric for example, also in References 15,31. Then the conclusion for non-conservative forces seems to be justified. However, a closer look has shown that in the connection with neighboring elements[31] or with physically reasonable boundary conditions, as discussed above and already pointed out in Reference 15, this unsymmetry is no longer present in the global load stiffness matrix.

The above-developed scheme is independent of the interpolation of the surface loaded with pressure. In all cases, stiffness matrices involving load terms are found. Interestingly, in the developments presented by Reference 36 working with higher order shell theory and curvilinear coordinates almost analytically the stiffness matrices–all, linear, quadratic and cubic parts–do not contain any pressure terms. Pressure is then only represented via the right-hand side, the load term; thus of course affecting the displacements of the shells reflected in the stiffness matrices. Large displacement analyses of plates and axisymmetric shells with bifurcation and post-buckling are presented for deformation dependent as well as independent pressure, confirming that the exact displacement formulation has to be taken for the deformation dependent load to achieve correct results. However, if eigenvalues are taken to determine bifurcation or limit points it is an open question, how far the missing stiffness-update parts are affecting the exact value.

4.2.1 | Solution algorithm

As already shown in References 19,21,37 without restriction of any kind, Equation (37) can be rewritten for one container–for simplicity only containing fluid–as follows:

$$[\mathbf{K}^* + b\ \mathbf{a} \otimes \mathbf{a}]\mathbf{d} = \mathbf{F} \tag{38}$$

with $\mathbf{K}^* = \mathbf{K}^{struct} + \mathbf{K}^f$ and $\mathbf{F} = \mathbf{f}^{ex} - \mathbf{f}^f - \mathbf{f}_{int}$.

According to Sherman-Morrison,[38,39] the solution to such a problem can be achieved by:

$$\mathbf{d} = \Delta\mathbf{u}_I - \beta\ \Delta\mathbf{u}_{II} \otimes \Delta\mathbf{u}_{II}\ \mathbf{F} \tag{39}$$

$$\text{with} \quad \Delta\mathbf{u}_I = \mathbf{K}^{*-1}\mathbf{F}, \quad \Delta\mathbf{u}_{II} = \mathbf{K}^{*-1}\mathbf{a} \quad \text{and} \quad \beta = \frac{b}{1 + b\ \mathbf{a} \cdot \Delta\mathbf{u}_{II}}. \tag{40}$$

Introducing Equations (40) into (39) the solution vector $\mathbf{d}$ can be obtained by one additional forward-backward substitution for the container plus two scalar products within the solution process using a direct solver:

$$\mathbf{d} = \Delta\mathbf{u}_I - \frac{b\ \Delta\mathbf{u}_{II} \cdot \mathbf{F}}{1 + b\ \mathbf{a} \cdot \Delta\mathbf{u}_{II}} \Delta\mathbf{u}_{II}. \tag{41}$$

It must be noted that in the input phase, a specification of all loaded surface segments, their relation to closed volumes, and their normal direction is necessary. Within the algorithm, the actual volume of the fluid in each container and the elements submerged by the fluid as well as the fluid level have to be computed to get the corresponding pressure correctly. The fluid level displacement in each iteration step is computed via:

$$\Delta u_w = \Delta\mathbf{u}_w \cdot \mathbf{w} = \frac{1}{S_t}\mathbf{a} \cdot \mathbf{d}. \tag{42}$$

For the rank-two-update of the stiffness matrix as given in Equation (37) the Sherman-Morrison procedure has to be applied recursively as it is standard for example, in the solution with Quasi-Newton solvers, see Reference 40 and for a vectorized version see Reference 41. For multiple containers within a general structure and different fillings, a major number of rank updates for at least parts of the global stiffness matrix including the load stiffness matrices have to be taken into account. The general recursive solution scheme and the implications for the computational requirements are described in detail by References 23,24.

4.3 | Discussion of some loading cases

4.3.1 | Further field definitions

Rotating structures containing fluids

A typical example of physically permissible cases is pressure loading due to a stationary rotation around an axis such as fluids in a centrifuge. However, in this scenario, the acceleration, which is radial, is no longer constant but linearly dependent on the current radius. Therefore, the above equations must be modified to combine gravitational acceleration with radial acceleration. Investigations regarding the rotation of thin membranes, including fluids, and their influence on stability can be found in Reference 42.

Magnetic fields

In magnetic fields, forces act on the masses of a structure with specific features. The forces are then dependent on the location of the specific masses in the magnetic field and, thus are deformation dependent, see for example, Reference 43 with application to a mass located on a cantilever beam. Also, a type of symmetric Hessian is obtained–a clearly conservative problem with conservative forces.

Space attached fields

In Reference 44 it was shown that in an arbitrary space attached "loading" field–in the specific case one way to model wind loading around a cylinder–symmetric global stiffness matrices are also obtained similar to the equations in a standard gravity field. The local magnitudes of the loading are then modified according to the deformation in this assumed field. As discussed above, the proper boundary conditions see Figure 9 have to be followed to achieve conservativeness. Such a type of loading field appears to be also possible by combining multiple magnetic fields with the gravity field. Whether these are physically reasonable situations has to be discussed.

4.3.2 | When considering deformation dependent loading, how and when not

Looking at the example in Figure 8 and considering a sphere under external pressure–no internal gas/air/fluid–thus the volume creating the external pressure would be very large, example *"a small structure in a large gas filled cylinder"*. Then only the normal change parts of Equation (18) for gas have to be taken and the corresponding FE load stiffness matrix plus the corresponding load residual part are obtained accordingly. For a stiff structure, this is particularly important for stability, as we know from analytical solutions for rings under compression that then the limit load is reduced by a quarter due to this follower force effect alone compared to not considering the normal change.

If the above example in Figure 8 of a *closed containment with internal fluid and gas or gas only* is itself embedded for example, in fluid and assuming this *outer fluid volume is rather large*, then in the FE model for the outer fluid only a load stiffness matrix and residual considering the normal change part have to be taken into account in addition, of course, integrated over the outer surface and with the correct sign.

A very direct example is to place for example, a *ship in a large volume of water*. Given the weight and the form of the structure, that is, the ship, the finite element modeling would only include the normal change part of the fluid over the wetted part of the structure with its residual and we would essentially end up with Archimedes' principle.

Though the radial deformations are not large in standard tanks for example, vertical *steel cylinders are filled with fluids, oil or water*, however, the deformation dependence of such a rather stiff structure is highly visible for axial loading, as the stability limits are increased with rising fluid level and internal gas pressure. It has proven to be important to simulate the complete filling process with fluid including the volume change to achieve the correct buckling loads and modes by accompanying eigenvalue analyses, for details see Reference 45.

The *stability analysis of shells* with (a) pure gas pressure support under some external loading–the latter representing a modified mass–or (b) by vacuum loading controlled by a piston motion is based concerning deformation dependent loading on the gas normal part of the stiffness matrix, the gas volume compression resp. reduction both represented by the rank-one update of the stiffness matrix and the corresponding residual term, see Reference 21. Combined with an arc-length solution scheme as described in section 5.1 the post-buckling path for both cases can be computed.

First steps of considering the *stability of shells* and obtaining post-buckling pathes under various deformation dependent loadings such as *fluid and wind* are presented already in References 46 and 16. However, volumetric effects were not taken into account in those studies. Additional research on shells involving fluid and gas plus their volumetric effects in arbitrary configurations is extensively discussed in Reference 24 and parts in References 23,45. Time integration is included to track the buckling of cylinders under external pressure or vacuum over time, as seen in References 47 and 48. These results appear to be particularly useful for design purposes.

Deformation dependence is not considered in applications with very high gas/air pressure such as *tires*, see Reference 49, due to the high pressure in the tires. For a review of tire models, see Reference 50 and of *air beams* see References 51–53 and 54,55. In the fairly simple *air beam models*, the cross-section is kept constant as also the internal pressure. However, the work of the internal pressure due to the volumetric deformation is considered in the overall virtual work expression. Thus, pressure terms also appear in the stiffness matrix, see for example, Reference 56. Wrinkling can be detected, but local effects such as localized Dirichlet boundary conditions leading to cross-section deformations cannot be taken into account limiting the applications to rather small deformations. In order to investigate problems with larger overall bending deformations a complete membrane tube discretized by finite elements and filled with gas has been studied–including all the terms derived for gas deformation dependence–showing strong local deformations of the cross-section at the support, see References 24,57. Such deformations indicate a general weakness of air-filled beam structures in practical applications.

For *membrane-type structures* with fluid filling and possible air support–see already a series of publications[58,59] and by Reference 60 for axisymmetric problems and also Reference 61–the volumetric terms of the load-stiffness matrix are essential, determining the fluid level. As the membranes are rather soft showing large deformations the nonlinear solution with the direct scheme as proposed in section 4.2, see equations (37) and following leads often to considerable convergence problems. In Reference 62 the authors propose and prove new robust algorithms with a particular focus on the volume constraint on various 3D ponding problems showing good efficiency and better convergence.

The *stability of thin membrane structures* considering fluid and/or gas filling based on the equations in section 4.2 is discussed in a series of papers.[63–66] A particular emphasis is on bifurcations and various post-buckling resp. post-bifurcation pathes.

Hydroforming is a commonly used metal forming technique mainly for ductile metals, see for some modeling schemes on tubes[67] and thin sheets.[68] The major advantage is that besides using simpler forming tools the final formed pieces show more equal wall thickness as problems with friction and sharp edges as found in stamping can be largely avoided.

A particular feature is that concavities can be formed. Concerning deformation dependence the normal change and the full volume constraint for fluid are considered and rather high pressures are taken. The forming process itself is typically divided into a low-pressure stage to adjust the formed part and a high-pressure stage for the actual forming, both with fairly high speed applied. However, inertia effects have no significance and time effects have only to be taken into account if viscous effects have to be considered.

As a resume of the above-cited examples deformation dependence of loading with its variations definitely depends on its use on one side as loading only or on the other side as "support" such as in closed containments as tires, balloons, rubber dams–see section 6–or membranes and structures filled with fluid. When used as quasi-external loading, only the normal dependence part must be considered. When considering the support situation, it is important to take into account the difference between heavy incompressible and compressible fluids or gas. In cases of combined loading such as a cylindrical tank filled with fluid and gas but also subjected to axial compression the stress stiffening in the structure caused by the filling is crucial for determining the buckling load compared to the normal change part of the stiffness.

5 | LOAD CONTROL IN NONLINEAR ANALYSIS

In nonlinear analysis, forces or moments are often increased or decreased in a logical manner when considering them as loading. The main objective is to determine limit loads for designing the corresponding structures. Whereas for Dirichlet boundary conditions a loading control can be clearly defined–though it may be hard to realize in real physics, the questionable use of forces or moments becomes apparent. Moments are definitely not a quantity that can act separately and forces can only be defined from masses in a gravitational field–for simplicity focussing on gravitation only. Therefore, it is not possible to increase or decrease their magnitude without further consideration. This means the model of loading control essentially controls masses, which should only be performed in a physically realistic manner. For pressure conditions, the pressure itself in statics is controlled through Dirichlet boundary modifications. This can be achieved by increasing or decreasing volumes through shape modifications, such as piston motion or adding gas or fluid, both quasi-statically.

In nonlinear static analysis, a common practice is to incorporate the structure's deformation or related quantities into the loading process to improve convergence in numerical analysis. The arc-length method is a standard approach. There a constraint involving one or more deformation quantities is added to the equilibrium equations. The solution of the combined system with the somehow augmented stiffness matrix can then be achieved either monolithically or sequentially, as suggested in the literature.[69–72] A fully monolithic solution scheme can raise the condition number of the linearized equation system to achieve better convergence and avoid singularities see Reference 73. However, when it comes to algorithms within a finite element program, it is much simpler to include arbitrary constraints in a sequential fashion. In the latter case, a practical observation is–see also Reference 74 that the ill-conditioning of the stiffness matrices has less of an effect on the solution than expected. Additionally, better convergence could of course be achieved by reducing the increase in loading magnitude, thus in turn reducing the corresponding arc length. Other suggestions are presented in Section 5.1.1.

5.1 | Arc length controlled loading on pressurized closed structures

The expression for the external virtual work of an external force $\mathbf{f}_{ext}$ with the control quantity for the load vector λ^{ext} and a pressure load which can be varied by a piston motion thus $v(\lambda^p)$ can be written as:

$$\delta\Pi_{ext} = \lambda^{ext}\mathbf{f}_{ext} \cdot \delta\mathbf{u} + \int_\eta \int_\xi p(\lambda^p)\, \mathbf{n} \cdot \delta\mathbf{u}\, d\xi d\eta. \tag{43}$$

The physical behavior of the enclosed gas is specified by Poisson's law.

$$pv^\kappa(\lambda^p) = PV^\kappa. \tag{44}$$

Introducing a path following algorithm to control the loading an arbitrary function of displacements and load level λ^{ext} resp. volume change factor λ^p is needed as a control law for the two separate load cases.

$$g(\mathbf{x}, \lambda) = 0 \qquad \text{with} \qquad \lambda = \lambda^{ext} \quad \text{or} \quad \lambda^p. \tag{45}$$

After the discretization of the virtual work expression with the virtual external work part $\delta\Pi_{ext}$ of Equation (43) and the additional Equations (44), (45) the linearization at state t for an incremental iterative procedure with the load level for the first case λ^{ext} as additional unknown yields:

$$\begin{bmatrix} \mathbf{K}^* + b\ \mathbf{a}\otimes\mathbf{a} & -\mathbf{P} \\ \mathbf{z}^T & \alpha \end{bmatrix} \begin{pmatrix} \mathbf{d} \\ \Delta\lambda^{ext} \end{pmatrix} = -\begin{pmatrix} \mathbf{R} - \lambda^{ext}\mathbf{P} \\ g \end{pmatrix}. \tag{46}$$

For simplicity $\mathbf{K}^* = \mathbf{K}_T - \mathbf{K}_{press}$ as stiffness matrix, $\mathbf{R} = \mathbf{f}_{int} - \mathbf{f}_{press}$ as residuum of the internal forces, and $\mathbf{P} = \mathbf{f}_{ext}$ as external force are introduced together. $b = \kappa\frac{p_t}{v_t}$ is the factor of the rank-one-update and the abbreviations for the directional derivatives are:

$$\mathbf{z} = \frac{d}{d\epsilon} g(\mathbf{x}_t + \epsilon\Delta\mathbf{u}, \lambda_t^{ext})|_{\epsilon=0} \tag{47}$$

$$\alpha = \frac{d}{d\epsilon} g(\mathbf{x}_t, \lambda_t^{ext} + \epsilon\Delta\lambda^{ext})|_{\epsilon=0}. \tag{48}$$

After the elimination of $\Delta\lambda^{ext}$ the problem is reduced into a pure displacement formulation.

$$\left[\mathbf{K}^* + b\ \mathbf{a}\otimes\mathbf{a} + \frac{1}{\alpha}\ \mathbf{P}\otimes\mathbf{z}\right]\mathbf{d} = -\left(\mathbf{F} + \frac{g}{\alpha}\mathbf{P}\right). \tag{49}$$

It is obvious that the global stiffness matrix $\mathbf{K}^*$ is finally updated by two rank-one matrices, a symmetric one for the gas pressure and a nonsymmetric one for the arc-length loading control. The right-hand side $\mathbf{F} = \mathbf{R} - \lambda^{ext}\mathbf{P}$ shows a modification due to the residual of the arc-length constraint equation. Applying the Sherman-Morrison formula four times the solution of the modified system of equations can be performed in the following fashion. First $\mathbf{d}$ is split into two parts via:

$$\mathbf{d} = \Delta\lambda^{ext}\ \mathbf{d}_I + \mathbf{d}_{II} \tag{50}$$

$$\text{with} \quad \mathbf{d}_I = [\mathbf{K}^* + b\ \mathbf{a}\otimes\mathbf{a}]^{-1}\mathbf{P}, \qquad \mathbf{d}_{II} = -[\mathbf{K}^* + b\ \mathbf{a}\otimes\mathbf{a}]^{-1}\mathbf{F}, \qquad \Delta\lambda^{ext} = -\frac{g + \mathbf{z}\cdot\mathbf{d}_{II}}{\alpha + \mathbf{z}\cdot\mathbf{d}_I}. \tag{51}$$

The interim solution vectors $\mathbf{d}_I$ and $\mathbf{d}_{II}$ are computed via:

$$\mathbf{d}_I = \mathbf{u}_I - \frac{b\ \mathbf{u}_{II}\cdot\mathbf{P}}{1 + b\ \mathbf{a}\cdot\mathbf{u}_{II}}\mathbf{u}_{II} \tag{52}$$

$$\mathbf{d}_{II} = -\mathbf{u}_{III} + \frac{b\ \mathbf{u}_{II}\cdot\mathbf{F}}{1 + b\ \mathbf{a}\cdot\mathbf{u}_{II}}\mathbf{u}_{II}. \tag{53}$$

$$\text{whereby} \quad \mathbf{u}_I = \mathbf{K}^{*-1}\mathbf{P}, \qquad \mathbf{u}_{II} = \mathbf{K}^{*-1}\mathbf{a}, \qquad \mathbf{u}_{III} = \mathbf{K}^{*-1}\mathbf{F} \tag{54}$$

While retaining the bandwidth of the stiffness matrix of the structure the solution vector $\mathbf{d}$ requires three forward backward substitutions within one step of the iterative solution process.

As a second case for a loading control a volume change is introduced like in a hydraulic system, then an arc-length controlled displacement can be assumed. In this case, the expression for the virtual work expression remains essentially unaltered. However, the control resp. constraint condition in Equation (45) is now composed for simplicity with $\lambda^{ext} = 0$ and nonconstant λ^p.

Thus the volume $v(\lambda^p)$ of the whole structure is decomposed into a deformable part and into a rigid part, see Figure 10. As a consequence the volume computation is separated into two terms, the deformable structure v_{struct} and the rigid structure, the piston volume v_{piston} with the piston surface s_{piston} and the piston motion $\lambda^p u_{ext}$.

$$v(\lambda^p) = v_{struct} + \lambda^p v_{piston} == \frac{1}{3}\int_\eta\int_\xi (\mathbf{x} - \mathbf{x}_0)\cdot\mathbf{n}\ d\xi d\eta + s_{piston}\lambda^p u_{ext}. \tag{55}$$

As shown above, the constraint for the control of the volume loading level λ^p and the displacement u_{ext} is:

$$g(\mathbf{x}, \lambda^p) = 0. \tag{56}$$

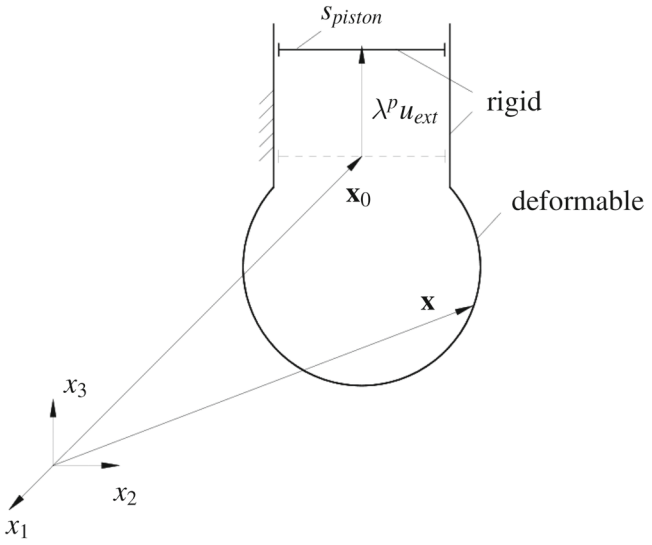

FIGURE 10 Volume computation; displacement controlled loading by piston motion.

Following the formal scheme as for pure load control as given in Equations (47), (48) the equation system becomes:

$$\begin{bmatrix} \mathbf{K}^* + b(\lambda_t^p)\ \mathbf{a} \otimes \mathbf{a} & -\mathbf{P}(\lambda_t^p) \\ \mathbf{z}^T & \alpha \end{bmatrix} \begin{pmatrix} \mathbf{d} \\ \Delta\lambda^p \end{pmatrix} = -\begin{pmatrix} \mathbf{R} \\ g \end{pmatrix} \tag{57}$$

$$\text{whereby} \qquad b(\lambda_t^p) = \frac{\kappa\ p_t}{v_t(\lambda^p)} \qquad \text{and} \qquad c = v_{piston} = s_{piston} u_{ext} \tag{58}$$

$$\text{and} \qquad v_t(\lambda^p) = \frac{1}{3} \sum_e \int_\eta \int_\xi (\mathbf{x}_t - \mathbf{x}_0) \cdot \mathbf{n}_t\ d\xi d\eta + \lambda_t^p v_{piston}. \tag{59}$$

$\mathbf{R} = \mathbf{f}_{int} - \mathbf{f}_{press}$ is the residuum of the quasi-internal forces and $\mathbf{P}(\lambda^p) = -b(\lambda^p)\ c\ \mathbf{a}$ is the vector of the quasi-external forces. An important difference to the situation shown above with external forces only, the vector of the quasi-external forces $\mathbf{P}(\lambda^p)$ is not linear concerning the control quantity λ^p. Finally, a further reduction of the system as shown in Equation (49) leads to the pure displacement formulation at state t.

$$\left[\mathbf{K}^* + b(\lambda_t^p)\ \mathbf{a} \otimes \mathbf{a} + \frac{1}{\alpha}\ \mathbf{P}(\lambda_t^p) \otimes \mathbf{z}\right] \mathbf{d} = -\left(\mathbf{R} + \frac{g}{\alpha}\mathbf{P}(\lambda_t^p)\right). \tag{60}$$

Computing the solution vector $\mathbf{d}$ via: $\qquad \mathbf{d} = \Delta\lambda^p\ \mathbf{d}_I + \mathbf{d}_{II}$

$$\text{with} \qquad \mathbf{d}_I = [\mathbf{K}^* + b\ \mathbf{a} \otimes \mathbf{a}]^{-1}\mathbf{P} \stackrel{!}{=} -b\ c\ [\mathbf{K}^* + b\ \mathbf{a} \otimes \mathbf{a}]^{-1}\mathbf{a} \tag{61}$$

$$\mathbf{d}_{II} = -[\mathbf{K}^* + b\ \mathbf{a} \otimes \mathbf{a}]^{-1}\mathbf{R} \tag{62}$$

$$\Delta\lambda^p = -\frac{g + \mathbf{z} \cdot \mathbf{d}_{II}}{\alpha + \mathbf{z} \cdot \mathbf{d}_I} \tag{63}$$

it can be seen that as a consequence of the direct dependence of the quasi-external load vector on the volume change only, two forward-backward substitutions within the iterative solution process are necessary. Then the interim solution vectors are

$$\mathbf{d}_I = -\frac{bc + 2b^2 c\ \mathbf{a} \cdot \mathbf{u}_{II}}{1 + b\ \mathbf{a} \cdot \mathbf{u}_{II}} \mathbf{u}_{II} \qquad \text{and} \qquad \mathbf{d}_{II} = -\mathbf{u}_{III} + \frac{\underline{b}\ \mathbf{u}_{II} \cdot \mathbf{R}}{1 + \underline{b}\ \mathbf{a} \cdot \mathbf{u}_{II}} \mathbf{u}_{II} \tag{64}$$

$$\text{with} \quad \mathbf{u}_{II} = \mathbf{K}^{*-1}\mathbf{a} \qquad \text{and} \qquad \mathbf{u}_{III} = \mathbf{K}^{*-1}\mathbf{R}. \tag{65}$$

Summarizing we obtain, that as demonstrated in the two examples for load cases loading control includes its own simulation model with many variations.

5.1.1 | Variations of arc-length control schemes

Firstly, it should be noted that a comprehensive description of the algorithm and corresponding program code is given in de Borst et al.[74]

In the literature, numerous variations of the original schemes can be found, with a fairly large number presented in a more recent contribution.[75] In addition to providing an overview, the authors also demonstrate the limits of load control algorithms including a factor for the load term and suggest a complete displacement control scheme that allows for the computation of arbitrary "load" deformation paths. The algorithm apparently adjusts the "load step" itself avoiding the need for too strong arc-length reductions necessary in other standard schemes. The authors also claim good efficiency for their new developments. A critical overview of the by-then available arc-length schemes is given by Reference 76 comparing the methods on some difficult post-buckling pathes involving snap-through and snap-back. The results show that some modifications of Crisfield's proposal,[71,77] the so-called spherical constraint–a nonlinear constraint–combined with the consistent linearization of the arc-length constraint, see Reference 78 led to a more robust scheme.

In standard Euclidean norms, which form the basis of arc-length algorithms mostly quantities with different units of measurement such as displacements, rotations, and load factors are summed. This introduces some arbitrariness into the algorithm. Scaling all quantities involved see Reference 79, for example, by their values obtained in an initial load step would avoid such an unbalanced operation. Combining the scaling with different factors could further allow to select dominant quantities and remove others.

At this point we recognize and have to note that the arc-length itself is not a physical quantity that can be realized to control the loading of practical structures for example, as controlling the occurrence of buckles in a cylinder under axial loading. The discussion of this aspect is further elaborated in section 5.2.

For very large problems the computational cost of a full Newton scheme can often be avoided by alternatives such as the modified Newton method or Quasi-Newton schemes. Then the characteristics of algorithms using arc-length schemes together with the modified Newton method can be largely improved by combining them with line search schemes, as pointed out by References 80 and 81. This is also applicable to a pure Newton method when large load steps have to be performed. Combining it with Quasi-Newton methods, where rank-updates are standard, can increase the solution's efficiency. Within the scheme, the deformation dependence modifies the stiffness matrix also by the vectorial updates, see References 46 and 41.

In damage and fracture mechanics, other controlling quantities are preferred to overcome the limit points advancing into a post-failure regime, see for example, References 82–86, and more recently.[87] All proposed schemes achieve fairly robust solutions even for so-called non-equilibrium paths.

5.2 | On applications of arc-length schemes–Merits–Limits–Implications for design

In addition to improving the convergence of the iterative algorithms for solving highly nonlinear problems with arc-length schemes, the latter schemes also allow for the computation of non-equilibrium states–which can be seen as their major merit. Nonlinear structural simulations using arc-length schemes often target failure points of structures, such as snap-through or bifurcation points in buckling and fracture. By the application of arc-length schemes, simply quasi-static behavior is assumed beyond these points often in non-equilibrium states or paths. Within these post-limit load deformation paths, we again encounter snap-back points and often also bifurcation points–see Figure 11.

The figure displays two load-displacement paths. The left side shows the result for an axially compressed cylinder under uniform loading, using a purely displacement based arc-length scheme and an adapted load step size in addition. The detail enlargement of the load-displacement path provides insight about the proximity of the so-called post-buckling load path giving an impression about the sequence of buckling modes occurring in the deformation process. The figure on the right[86] shows the results for a plane strain sheet loaded with uniform tensile loading by prescribed displacement on one side, fixed on the other, with cracks developing. The applied arc-length algorithm incorporates therefore fracture quantities with step-size adjustment to capture material failure thus crack evolution in a quasi-sequential fashion. The fracture process is represented by a rather complex curve with a zig-zagging of the loading displacement in the post-failure regime.

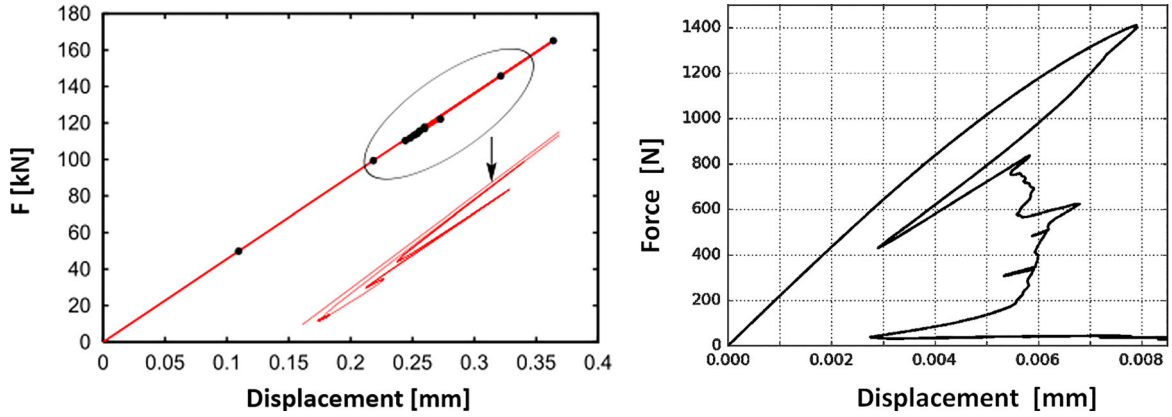

FIGURE 11 Typical load displacement diagrams with snap-through and snap-back points. Left: Loading and post-buckling pathes for a cylinder under longitudinal compression loading. Right: Fracturing of a tensile loaded specimen[86]–post-failure path obtained with fracture-based path following scheme fully capturing crack evolution.

An argument to compute post-limit parts of load-displacement curves is the goal of gaining knowledge about the lowest points or branches of equilibrium in the post-limit regime. Such results could then possibly be used for design purposes such as determining the lowest allowed load level, often called design level. However, applications of post-buckling analysis, such as for longitudinally loaded cylinders, are extremely cumbersome and have shown no reliable results, as for real structures such as cylindrical shells many post-buckling branches have to be followed. This particular aspect is visible in the post-failure path for example, in Figure 11 left. Obviously, this path closely follows the initial loading path, however, in the opposite direction, indicating somehow the sensitivity of the current equilibrium state on the original path to any perturbation, whether due to changes in the geometry or unexpected dynamic loading or similar. We also recognize that there may be multiple equilibrium or non-equilibrium paths that are closely situated to each other, depending on the decision made at the bifurcation point to follow one branch or the other. Therefore, the general idea of path-following appears then to be rather questionable.

For fracture problems, post-failure paths are determined by the sequential failure of various structural parts, mostly following cracks that may also show branches. Again decisions have to be made on which branch to follow. The major advantage of this fracture-following scheme is obtaining a sequence in the fracture and crack evolution process. This may have some influence on a design, however the academic interest in the material fracture modeling and the appropriate algorithms themselves appears to dominate often. Besides that, the practical realization of such a quasi-static post-failure processes is definitely difficult even in laboratory experiments.

Thus, the following question remains for all problems computed with one or the other arc-length algorithm in a post-limit regime: Is the assumption of statics in any post-limit path still justified, thus no inertia effects and no dependencies of material quantities on velocity and even no effects of sudden contacts?

For many designs, it might then be more beneficial to apply dynamic perturbation and look at the time history behavior to obtain the sensibility of a pre-buckling or pre-failure state against for example, a kinetic perturbation, see References 47,48. However, investigations concerning the choice of the perturbation are then necessary, certainly individually and reflecting real uncertainties for the considered type of structure and loading.

5.3 | On physically controversial loading models

Although many models proposed in the literature are mathematically correct, they may not be physically workable and cannot be realized in experiments.

A physically rather controversially discussed example with large deformations–rolling a strip into itself under an applied moment–see section 3.2 and Figure 5–is shown in many contributions on FE technology. However, it cannot be realized with certainty in any experiment. Following the arguments in section 4.1.4 concerning boundary conditions, we have clearly a nonsymmetric load-stiffness matrix and nonconservative loading for the distributed loading acting on the beam Figure 5 left. Even for the single follower loads representing the moment loading the corresponding load stiffness terms will be nonsymmetric–also a nonconservative loading.

However, a finite element model mathematically correct and even showing fully symmetric tangent matrices has been constructed as the inverse application of a developed geometrically exact computational contact mechanics model, see Reference 88. The contact forces normally arising from the interaction between bodies–here a body is assumed to contact at the right end of the beam–are considered to model the effect of follower forces and are displayed in Figure 5. A contradictory observation at first look, however, in contact analysis the other boundary should also to be taken into account. Therefore, the assumed load is not a completely independent follower force type loading, rather an interaction force quantity. Nevertheless, it is unclear, how the contacting body has to be moved to achieve the moment loading during the full loading process. Essentially, the loading process is shifted one step further "outside" the directly considered beam problem.

The same consideration could be followed to model either follower force by contacting bodies, the latter controlled by undefined devices. The specific motion of such devices could be obtained through reverse analysis–not a practically relevant procedure.

When discussing the physical realization of standard load control on a structure–no gas, no fluid, ist is essential that masses are controlled and, therefore modified. For a single mass, this is equivalent to a single point load and can be easily realized. However, for arbitrarily distributed masses represented by more or less uniformly distributed loading in a simulation model the physical realization is more complex. Assuming von Neumann boundary conditions, a flexible boundary loaded by an increasing distributed mass would require fairly stiff 'upper' constructions in real physical structures to carry and distribute the higher mass, thus as a consequence representing a different boundary condition. A typical example is the analysis of cylinders under axial uniform loading, for which–interestingly–lower buckling loads are computed than observed in experiments. This is not unexpected as such a loading cannot be realized. The experiments, however, are either displacement-driven or by hydraulic devices with mostly imperfect contact conditions between the loading plate and cylinder.

6 | RUBBER DAMS AS A SPECIFIC STRUCTURE WITH BOTH–SUPPORT AND LOADING BY AIR AND/OR FLUID

In addition to balloons, air domes, and general inflatable structures, rubber dams are a well accepted but not too often implemented building instrument in engineering, particularly in river management. They are a very important alternative to steel weirs, as the art of manufacturing steel weirs for smaller rivers becomes too costly nowadays. Even repairing becomes difficult, as finding competent craftsmen and companies can be a challenge, even in highly industrialized countries. As the author's group had the opportunity to work on such projects from the basic analysis to the design with the German Federal Waterways Engineering and Research Institute in Karlsruhe, the topic will be presented in a broader context, including general design information. For a detailed technical overview of these structures, please refer to the PIANC report InCom WG166 from 2018.[89]

Rubber dams are simply described as tubes positioned horizontally, fixed to the ground and on both ends of the tube. The walls of the tube are very flexible; some look almost like thin membranes, however, the reality obtained by the author's group was tube walls with quite some bending stiffness due to a wall thickness of 10–15 mm of layered material. A cost advantage of rubber dams is the simple construction see Figure 12, as after manufacturing the multilayer-ply material as a long plane sheet is put to the ground, then bent into a tube shape, and fixed to the bottom. It is important to ensure the fixation is strong enough, the connections are tight and impermeable to air and water. The fixations should also provide full buoyancy control, especially for air-filled dams. The simple basic construction principle causes difficulties at both ends of the tube, where proper fixation to the side walls is necessary. This may have the consequence of some wrinkles, but folds should be avoided. A selective design can help optimize this issue, as discussed below.

First, the general cross-section of the dam has to be found based on the given dam height and on requirements within the later dam operation. The initial design typically involves analytical solutions, such as two-dimensional models that incorporate air and fluid filling for example, References 91–93. Upon comparison, the analytical solution only differs rather slightly within ranges of higher pressure from finite element solutions. However, at lower pressures the FE solutions show some deviations particularly due to difficulties of the analytical solutions capturing the deformed shape, see References 90,94 for a number of studies and also Reference 24. Full water-filled dams exhibit minimal cross-section deformation within variations of head and bottom water. However, proper fixation of the tube at the bottom has to be provided–see Figure 13, where it becomes visible for the example of full air filling that the cross section and as a consequence the dam height is not kept constant during the loading process. The simulation model for fluid and gas loading

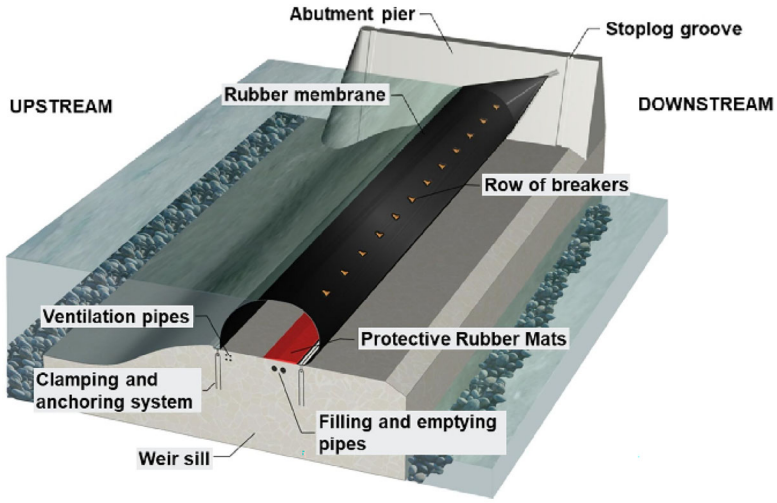

FIGURE 12 Rubber dam. General construction. For details see Gebhardt et al.[90]

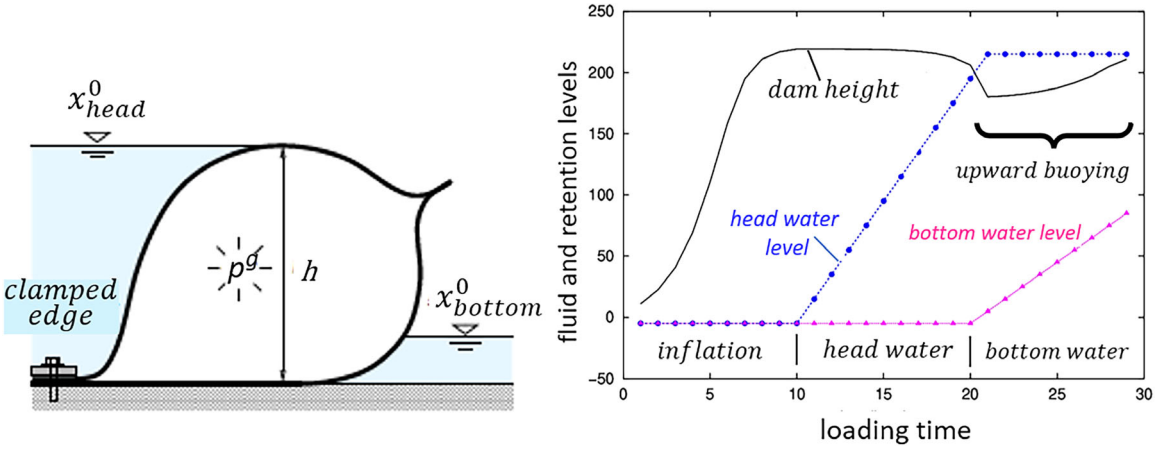

FIGURE 13 Rubber dam, single fixation (left). Loading process of air filled dam (right). Form changes due to uplift.

consists of three chambers, see References 23,24, each controlled separately according to the solution scheme provided in section 4. The first chamber is the inner tube, which is filled with air by adding gas volume. The other two chambers, representing the upstream resp. the downstream water are fluid filled each by adding fluid volume separately, effectively adding volume through piston motion.

Thus after folding the tube, first the internal filling is performed. Then, the upstream (head) water level rises to the full dam height, followed by an increase in the level of the downstream (bottom) water, see Figures 13 and 14 right. Without a second fixation, the cross section deforms undesirably due to uplift, see Figure 13 right, which is known as upward buoying caused by downstream water. However, when fixed at the bottom water side–as shown in Figure 14 left, the shape is perfectly maintained and no buoying is observed when the bottom water rises, see Figure 14 right. The same critical buoyancy behaviour for a tube without second fixation is found for the cases of water and a combined water plus air filling of the tube, if the water filling level is not sufficiently high, see References 24,95.

The optimal solution for preventing major deformations is achieved by fully filling the dams with fluid. However, partial or full air filling allows for a faster and simpler operation, such as fairly quickly lowering the dam height. On the other side, air-filled dams are susceptible to buckling as a consequence of compressible air. To prevent this, either very high air pressure should be used or the level of fluid filling should be kept reasonably high. Three-dimensional analyses using rather large FE models, following the three-chamber model described above were necessary for buckling investigations, see Reference 24 and particularly for avoiding large folds in the boundary region of the dams, see Figures 15 and

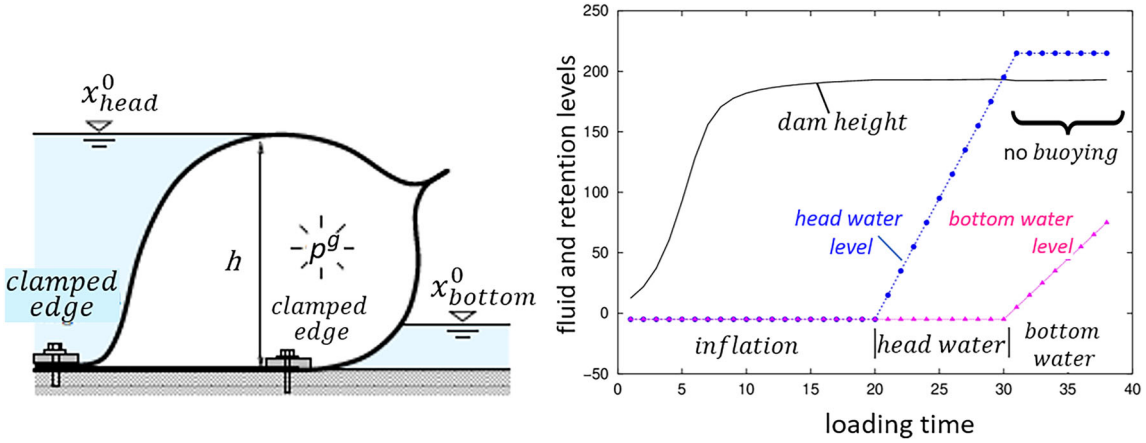

FIGURE 14 Rubber dam within double fixation (left). Loading process of air filled dam (right) fixation. Uplift avoided–no buoying.

FIGURE 15 Rubber dam. Undesirable fold at abutment pier–major head water loss.

16. These folds are caused by the type of connection at the side walls, the abutment piers. They are prone to considerable undesired water loss and can be largely avoided by careful design. Varying several parameters such as the slope of the abutment pier, the angles of the clamping rails for the rubber sheet at the abutment pier in correlation with the chosen cross-section a comprehensive series of finite element analyses was performed, initiated by the German Federal Waterways Engineering and Research Institute Karlsruhe, see References 90,96–98 to obtain optimal results limiting or almost avoiding folds. In Figure 17 three typical results varying the connection at and the deflection of the abutment pier are shown, proving that folds can degenerate into rather small wrinkles. However, the choice of such "optimal" parameters is subject to local construction limitations. For additional design aspects and simulations, refer to Reference 99. A final study, described in References 90,100, was on the potential damage to the rubber material caused by debris impact in the head water or any type of vandalism, such as knife attacks or gunshots. The simulations for dams with air or fluid filling impacted by a tree model with a fairly sharp edge, different velocities and different angles of attack conducted with Reference 11 showed no significant damage. The use of air filling resulted in a perfect elastic response, while fluid filling resulted in almost no elastic response. However, the stresses in the dam skin were well below any expected damage level in both cases. Nevertheless, further simulations revealed that too low air pressure causes large deformation and higher stresses in the rubber material. A clear sign, that the air pressure level should be maintained at a high level, which is also beneficial to prevent buckling. A further observation in Reference 100 is that air-filled dams are more sensitive to minor holes than fluid-filled ones, because air loss evolves rather quickly, whereas water outflow is not as dramatic for such holes. The chosen multi-ply material at holes prevents fracture propagation and these mostly small holes can be easily repaired.

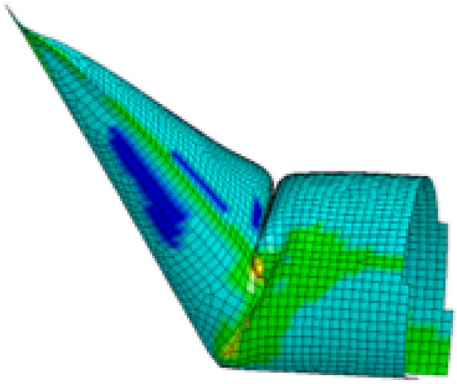

FIGURE 16 Simulation with finite elements–Clear fold development due to connection at abutment pier.

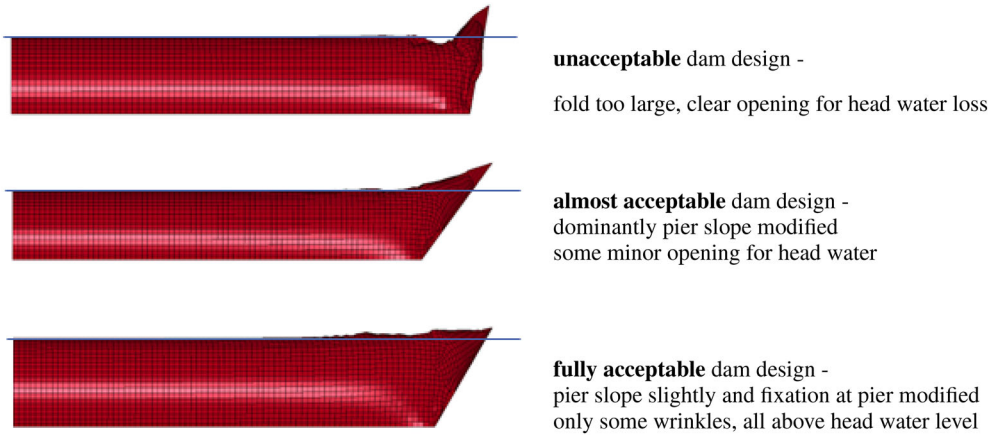

FIGURE 17 Design investigation by parameter variation (different fixation at and slope of abutment pier) to avoid or minimize folds.

7 | CONCLUSIONS

Based on the discussion in section 3, it is recommended that load modeling and simulation in nonlinear static analysis follow the same approach as for a dynamic simulation. Besides material and geometry, the focus should be on the idea of mass modifications simulating an increasing load within a gravitation field or similar. It must be noted that classical modifications of Dirichlet boundary conditions are not affected by the discussion in this contribution.

When attempting to find a suitable load model in nonlinear static analysis for challenging scenarios, such as wind loading or interaction with other media like sand or gravel, it is important to avoid introducing artificial effects through load modeling assumptions. The latter is often obtained in the "follower force" literature.

The formal developments of pressure loading resulting from gas/fluid media interacting with structures either as support or as loading show the expected results concerning boundary conditions and conservativeness of the loading for physically permissible constructions. The need for taking into account the various deformation-dependence terms of the developed formulations in an FE simulation depends much on the structure in focus. This may serve also as a basis for simplified formulations and FE analyses.

Furthermore, performing load control with additional constraints such as arc-length methods is certainly a viable tool to improve convergence, as in principle the stiffness matrix is updated by a rank-one matrix due to the accompanying arc-length control, see References 73 and 78. However, in realistic cases, the structural behavior beyond limit points is dynamic and involves at least some inertia resulting in kinetic effects. This behavior is mostly accompanied by structural failure, such as buckling, fracturing, or large plastic deformations. Therefore, the idea of computing quasi-static post-limit load-deflection curves appears to be meaningless for standard structures with complex loading, particularly for design purposes. In cases where the determination of the failure process is vital, it is important to consider the dynamic behavior of the structure by nonlinear transient analysis.

The final investigations on rubber dams, conducted in cooperation with the German Federal Waterways Engineering and Research Institute (BAW), demonstrated the wide range of applications of the developments for modeling gas and fluid loading in nonlinear statics, including buckling and contact analysis.

ACKNOWLEDGMENT

Open Access funding enabled and organized by Projekt DEAL.

DATA AVAILABILITY STATEMENT

The data that support the findings of this study are available from the corresponding author upon reasonable request.

ENDNOTES

*Though flutter is purely a dynamic phenomenon known in aircraft design, in the literature devoted to stability the term flutter has been introduced in structures with specific combinations of loading leading to instability.

†In our contribution we prefer to mark the state with t letter though in many numerical realizations t belongs to the natural set numbers that is, $\{0, 1, 2, \ldots\}$.

ORCID

Karl Schweizerhof https://orcid.org/0009-0000-5815-5257

Alexander Konyukhov https://orcid.org/0000-0002-4172-5396

REFERENCES

1. Eurocode 1. Actions on structures–EN 1991 Part 1.1-1.7 and parts 2-5: General actions as well as e.g. traffic loads on bridges and other civil engineering works. 2021.
2. Beck M. Die Knicklast des einseitig eingespannten, tangential gedrückten Stabes. (in German). *Z Angew Math Phys*. 1952;3:225-228.
3. Pflüger A. Zur Stabilität des tangential gedrückten Stabes. *Z Angew Math Mechanik*. 1955;35:191.
4. Ziegler H. Die Stabilitätskriterien der Elastomechanik. *Ingenieur-Archiv*. 1952;20:49-56.
5. Bolotin VV. *Nonconservative Problems in the Theory of Elastic Stability*. Fizmatgiz Publishers, Moscow (in Russian) 1961. Pergamon Press; 1963 English translation.
6. Koiter WT. Unrealistic follower forces. *J Sound Vib*. 1996;194:636-638.
7. Herrmann G. Dynamics and stability of mechanical systems with follower forces. NASA Technical Report No. NASA CR-1782 1971.
8. Elishakoff I. Controversy associated with the so-called "follower forces": critical overview. *Appl Mech Rev*. 2005;58:117-142.
9. Bigoni D, Kirillov ON, Misseroni D, Noselli G, Tommasini M. Flutter and divergence instability in the Pflüger column: experimental evidence of the Ziegler destabilization paradox. *J Mech Phys Solids*. 2018;116:99-116.
10. Oldfather WA, Ellis CA, Brown DM. Leonhard Euler's elastic curves. *Isis*. Vol 20. The University of Chicago Press, The History of Science Society; 1933:72-160. http://www.jstor.org/stable/224885
11. Hallquist JO, Tsay CS. LS-DYNA theoretical manual. *Nonlinear Dynamic Analysis of Structures Vs. 950*. Livermore Software Technology Corporation; 2000.
12. Pearson CE. General theory of elastic stability. *Quart Appl Math*. 1956;14:133-144.
13. Sewell MJ. On configuration-dependent loading. *Arch Rational Mech Anal*. 1966;23:327-351.
14. Romano G. Potential operators and conservative systems. *Meccanica*. 1972;7:141-146.
15. Schweizerhof K, Ramm E. Displacement dependent pressure loads in nonlinear finite element analyses. *Comput Struct*. 1984;18:1099-1114.
16. Schweizerhof K, Ramm E. Follower force effects on stability of shells under hydrostatic loads. *ASCE J Eng Mech*. 1987;113:72-88.
17. Simo JC, Taylor RL, Wriggers P. A note on finite element implementation of pressure boundary loading. *Commun Appl Numer Methods*. 1991;7:513-525.
18. Berry D, Yang H. Formulation and experimental verification of a pneumatic finite element. *Int J Numer Methods Eng*. 1996;39:1097-1114.
19. Bonet J, Wood RD, Mahaney J, Heywood P. Finite element analysis of air supported membrane structures. *Comput Methods Appl Mech Eng*. 2000;190:579-595.
20. van Dijk R, van Keulen F, Sterk J. Simulation of closed thin-walled structures partially filled with fluid. *Int J Solids Struct*. 2000;37:6063-6083.
21. Rumpel T, Schweizerhof K. Volume dependent pressure loading and its influence on the stability of structures. *Int. J. Numer. Methods Eng.* 2003;56(2):211-238.
22. Rumpel T, Schweizerhof K. Hydrostatic fluid loading in non-linear finite element analysis. *Int J Numer Methods Eng*. 2004;59:849-870.
23. Haßler M, Schweizerhof K. On the static interaction of fluid and gas loaded multi-chamber systems in large deformation finite element analysis. *Comput Methods Appl Mech Eng*. 2008;197(19):1725-1749.
24. Haßler M. *Quasi-Static Fluid-Structure Interactions based on a Geometric Description of Fluids, (in English)*. PhD thesis. University Karlsruhe; 2009.

25. Rumpel T. *Effiziente Diskretisierung von statischen Fluid-Struktur-Problemen bei großen Deformationen, (in German)*. PhD thesis. University Karlsruhe; 2003.
26. Bufler H. Pressure loaded structures under large deformations. *Zamm*. 1984;64(7):287-295.
27. Bufler H. Zur Potentialeigenschaft der von einer Flüssigkeit herrührenden Druckbelastung. *Zamm*. 1985;65(4):130-132.
28. Bufler H. Konsistente und nichtkonsistente Druckbelastungen durch Flüssigkeiten. *Zamm*. 1992;72(7):T172-T175.
29. Bufler H. Configuration dependent loading and nonlinear elastomechanics. *Zamm*. 1993;73(4-5):T20-T33.
30. Fisher D. Conservative configuration dependent loads on bounded surfaces. *Zamp*. 1987;38:883-892.
31. Hibbitt HD. Some follower forces and load stiffness. *Int J Numer Methods Eng*. 1979;14:937-941.
32. Knebel K. *Stability of steel cylinders with unilateral boundary conditions under static and dynamic loading. (in German)*. PhD thesis. University Karlsruhe; 1997.
33. Hoareau C, Deü J-F. Nonlinear equilibrium of partially liquid-filled tanks: a finite element/level-set method to handle hydrostatic follower forces. *Int J Non-Linear Mech*. 2019;113:112-127. doi:10.1016/j.ijnonlinmec.2019.03.014
34. Qing Q, Pang Y, Tang T, Ji T, Gong J. Loading-shape interaction analysis of membrane structures subjected to deformation dependent hydrostatic loadings. *Thin-Walled Struct*. 2023;189:110782.
35. Rumpel T, Schweizerhof K, Gebhardt M. On an efficient model for the inflation and loading process of gas and fluid supported membrane and shell structures. In: Onate E, Kröplin B, eds. *Textile Composites and Inflatable Structures*. CIMNE; 2003:316-322.
36. Amabili M, Breslavsky I. Displacement dependent pressure load for finite deflection of doubly-curved thick shells and plates. *Int J Non-Linear Mech*. 2015;77:265-273.
37. Rumpel T, Schweizerhof K. Volume dependent pressure loading and large deformation finite element analysis of structures. In: Wall W, Bletzinger K, Schweizerhof K, eds. *Trends in Computational Structural Mechanics*. CIMNE; 2001:386-396.
38. Sherman I, Morrison WI. Adjustment of an inverse matrix corresponding to changes in the elements of a given column or a given row of the original matrix. *Ann Math Stat*. 1947;20:621.
39. Zielke H. Inversion of modified symmetric matrices. *J Assoc Comput Mach*. 1968;15:402-408.
40. Matthies H, Strang G. The solution of nonlinear finite element equations. *Int J Num Methods Eng*. 1979;14:1613-1626.
41. Schweizerhof K, Hallquist JO. *Vectorized Quasi-Newton Methods for Nonlinear Structural Analysis Combined with Path-Following Algorithms. Part I*. Institut für Baustatik, University Karlsruhe; 1989 Available via researchgate.
42. Zhou Y, Nordmark A, Eriksson A. Instability investigation for rotating thin spherical membrane. *Int J Non-linear Mech*. 2017;97:96-106.
43. Mok DP, Wall WA, Bischoff M, Ramm E. Algorithmic aspects of deformation dependent loads in non-linear static finite element analysis. *Eng Comput*. 1999;16(5):601-618.
44. Schweizerhof K. *Nonlinear analysis of structures under deformation dependent loading using finite elements*. PhD thesis. University Stuttgart; 1982 (in German).
45. Haßler M, Schweizerhof K. On the influence of fluid-structure interaction on the static stability of thin walled shell structures. *Int J Struct Stab Dyn*. 2007;7(2):313-335.
46. Ramm E, Schweizerhof K, Stegmüller H. Ultimate load analysis of thin shells under pressure loads. In: Bergan PG, Bathe KJ, Wunderlich W, eds. *Europe-US Symposium 'Finite Element Methods for Nonlinear Problems', Trondheim, Norway, 1985. Proceedings*. Springer-Verlag; 1986:339-357.
47. Ewert E, Schweizerhof K, Vielsack P. Measures to judge the sensitivity of thin-walled shell structures concerning stability under different loading conditions. *Proceedings WCCM VI World Congress on Computational Mechanics 2004*. Vol 37. Tsinghua University Press & Springer Verlag; 2004:507-522.
48. Ewert E. *Stabilitäts und Sensitivitätsuntersuchungen dünnwandiger Kreiszylinder unter axialem und radialem Druck mit der Methode der Finiten Elemente*. (in German) PhD thesis. University Karlsruhe; 2008.
49. Kennedy R, Padovan J. Finite element analysis of steady and transiently moving/rolling nonlinear viscoelastic structure-II. Shell and three-dimensional simulations. *Comput Struct*. 1987;27(2):259-273.
50. Wang Y-S, Cui Z-B, Wu J. *A Review of the Models for Pneumatic Tire Stres Analysis*. LAP Lambert Academic Publishing; 2017.
51. Wielgosz C, Thomas JC, Casari P. Strength of inflatable fabric beams at high pressure. Paper presented at: AIAA/ASME/ASCE/AHS Structures, Structural Dynamics and Material Conference, Denver. 2002 43:1292.
52. Thomas JC, Wielgosz C. Deflections of highly inflated fabric tubes. *Thin-Walled Struct*. 2004;42:1049-1066.
53. van Le A, Wielgosz C. Bending and buckling of inflatable beams: some new theoretical results. *Thin-Walled Struct*. 2005;43:1166-1187.
54. Riches CG, Gosling PD. Numerical analysis of the load-deflection characteristic of pneumatic beam structures. Proceedings of the IASS International Congress'98, Lightweight Structures in Architecture, Engineering and Construction. 1998 2:883–894.
55. Riches CG, Gosling PD. Pneumatic structures: a review of concepts, applications and analytical methods. Proceedings of the IASS International Congress'98, Lightweight Structures in Architecture, Engineering and Construction. 1998 2:874–882.
56. Davids WG, Zang H. Beam finite elements for nonlinear analysis of pressurized fabric beam-columns. *Eng Struct*. 2008;30:169-1980.
57. Haßler M, Schweizerhof K. Validation and limits of finite inflatable beam elements. *PAMM Proc Appl Math Mech*. 2008;8(1):10283-10284.
58. Szyszkowski W, Glockner P. Finite deformation and stability behaviour of spherical inflatables subjected to axi-symmetric hydrostatic loading. *Int J Solids Struct*. 1984;20(11-12):1021-1036.
59. Stanuszek M, Glockner P. Further results of spherical inflatables under axisymmetric hydrostatic loads. *Comput Struct*. 1995;57:35-45.
60. Tuan CY. Ponding on circular membranes. *Int J Solid Struct*. 1998;35(3-4):269-283.
61. Katsikadelis JT, Nerantzaki MS. The ponding problem on elastic membranes: an analogue equation solution method. *Comput Mech*. 2002;28:122-128.

62. Narayanana NK, Wüchner R, Degroote J. Monolithic and partitioned approaches to determine static deformation of membrane structures due to ponding. *Comput Struct*. 2021;244:106419.
63. Zhou Y, Nordmark A, Eriksson A. Instability of thin circular membranes subjected to hydro-static loads. *Int J Non-linear Mech*. 2015;76:144-153.
64. Zhou Y, Nordmark A, Eriksson A. Multi-parametric stability investigation for thin spherical membranes filled with gas and fluid. *Int J Non-linear Mech*. 2016;82:37-48.
65. Zhou Y, Nordmark A, Eriksson A. Multi-parametric stability investigation for thin spherical membranes with contacts. *Int J Mech Sci*. 2017;131-132:334-344.
66. Zhou Y. *Numerical Instability Investigations for Thin Membranes*. KTH Royal Institute of Technology. Doctoral thesis in Engineering Mechanics, Stockholm; 2017.
67. Tran K. Finite element simulation of the tube hydroforming process-bending, preforming and hydroforming. *J Mater Process Technol*. 2002;127:401-408.
68. Hatipoglu HA, Polat N, Köksal A, Tekkaya AE. Modeling flexforming (fluid cell forming) process with finite element method. *Key Eng Mater*. 2007;344:469-476.
69. Wempner GA. Discrete approximations related to nonlinear theories of solids. *Int J Solids Struct*. 1971;7:1581-1599.
70. Riks E. The application of Newton's method to the problem of elastic stability. *J Appl Mech*. 1972;39:1060-1066.
71. Crisfield MAA. Faster modified Newton-Raphson iteration. *Comput Methods Appl Mech Eng*. 1979;20:267-278.
72. Ramm E. Strategies for tracing the nonlinear response near limit points. In: Wunderlich W, Stein E, Bathe KJ, eds. *Nonlinear Finite Element Analysis in Structural Mechanics*. Springer; 1981:63-89.
73. Keller HB. Practical procedures in path following near limit points. In: Glowinski R, Lions J-L, eds. *Computing Methods in Applied Sciences and Engineering*. North-Holland; 1982.
74. Borst R de, Crisfield MA, Remmers JJC, Verhoosel CV. *Non-Linear Finite Element Analysis of Solids and Structures*. J. Wiley &Sons; 2012.
75. Pretti G, Coombs WM, Augarde CE. A displacement-controlled arc-length solution scheme. *Comp Struct*. 2022;258:106674.
76. Carrera E. A study on arc-length-type methods and their operation failures illustrated by a simple model. *Comput Struct*. 1994;50(2):217-229.
77. Crisfield MAA. Fast incremental/iterative solution procedure that handles snap-through. *Comput Struct*. 1981;13:55-62.
78. Schweizerhof K, Wriggers P. Consistent linearization for path following methods in nonlinear finite element analyses. *Comput Methods Appl Mech Eng*. 1986;59:262-279.
79. Simo JC, Wriggers P, Schweizerhof K, Taylor RL. Finite deformation post-buckling analysis involving inelasticity and contact constraints. In: Liu WK, Belytschko T, Park KC, eds. *Proceedings of the Int. Conf. "Innovative Methods for Nonlinear Problems"*. Pineridge Press; 1984:365-387.
80. Crisfield MA. An arc-length method including line searches and accelerations. *Int J Numer Methods Eng*. 1983;19:1269-1289.
81. Schweizerhof K. Consistent concept for line search algorithms in combination with arc-length constraints. *Commun Appl Numer Methods Eng*. 1993;9:773-784.
82. de Borst R. Computation of post-bifurcation and post-failure behaviour of strain-softening solids. *Comput Struct*. 1987;25:521-539.
83. Geers M. Enhanced solution control for physically and geometrically nonlinear problems. Part ii-comparative performance analysis. *Int J Numer Methods Eng*. 1999;46(2):205-230.
84. Geers M. Enhanced solution control for physically and geometrically nonlinear problems. Part i-the subplane control approach. *Int J Numer Methods Eng*. 1999;46(2):177-204.
85. Verhoosel CV, Remmers JJC, Gutiérrez MA. A dissipation-based arc-length method for robust simulation of brittle and ductile failure. *Int J Numer Methods Eng*. 2009;77(9):1290-1321.
86. Singh N, Verhoosel CV, De Borst R, Van Brummelen EH. A fracture-controlled path-following technique for phase-field modeling of brittle fracture. *Finite Elem Anal Des*. 2016;113:14-29.
87. Bharali R, Goswami S, Anitescu C, Rabczuk T. A robust monolithic solver for phase-field fracture integrated with fracture energy based arc-length method and under-relaxation. *Comput Methods Appl Mech Eng*. 2022;394:114927.
88. Konyukhov A. General descriptions of follower forces derived via a geometrically exact inverse contact algorithm. *Int J Numer Methods Eng*. 2016;108(11):1290-1306. doi:10.1002/nme.5253
89. PIANC. The World Association for Waterborne Transport and Infrastructure. Inflatable structures in hydraulic engineering, PIANC Report "InCom WG 166". 2018.
90. Gebhardt M, Maurer A, Schweizerhof K. On the hydraulic and structural design of fluid and gas filled inflatable dams to control water flows in rivers. In: Onate E, ed. *Structural Membranes 2011, Vth Int. Conf. On Textile Composites and Inflatable Structures, Proceedings*. CIMNE; 2011:374-384.
91. Anwar HO. Inflatable dams. *J Hydraul Div ASCE*. 1967;93(Hy3):99-119.
92. Harrison HB. The analysis and behavior of inflatable dams under static loading. *Proc Inst Civil Eng*. 1970;45:661-676.
93. Ministry of Land, Infrastructure and Transport (MLIT), River Bureau, Japan. Technical guidelines for Rubberdams, Translation from Japanese – German Federal Waterways Engineering and Research Institute in Karlsruhe (BAW) Unpublished. 2000.
94. Gebhardt M. *Hydraulische und Statische Bemessung von Schlauchwehren, (in German)*. PhD thesis. University Karlsruhe; 2006.
95. Haßler M, Schweizerhof K. Nonlinear finite element analysis of inflatable prefolded membrane structures under hydrostatic loading. In: Onate E, Kröplin B, eds. *Textile Composites and Inflatable Structures II*. CIMNE; 2005:83.

96. Maurer A, Gebhardt M, Schweizerhof K. Computation of fluid and/or gas filled inflatable dams. Proceedings 8. LS-DYNA Anwenderforum Bamberg2010, DYNAmore GmbH, Stuttgart. 2010.
97. Gebhardt M, Maurer A, Schweizerhof K. Schlauchwehre: Zur Formfindung, Berechnung Und Bemessung der Membran. Kolloquium Innovation Mit Tradition: Hydraulischer Entwurf Und Betrieb von Wasserbauwerken, Proceedings, German Federal Waterways Engineering and Research Institute in Karlsruhe (BAW). 2012.
98. Maurer A, Gebhardt M, Schweizerhof K. Finite-Elemente-Analysen zur Optimierung der Geometrie und der Spannungsverteilung in der Membran von Schlauchwehren. 35. Dresdner Wasserbaukolloquium 2012, "Stahlbauwerke-Planen, Bauen, Betreiben", Proceedings TU Dresden, Dresdner Wasserbauliche Mitteilungen 47. Dresden: Technische Universität Dresden, Institut für Wasserbau und technische Hydromechanik. 2012 47:473-482. (in German).
99. Gurt R, Deutscher M, Gebhardt M. Design and analysis of reinforced rubber membranes for inflatable dams. In: Oñate E, Bletzinger K-U, Kröplin B, eds. *Proceedings VII International Conference on Textile Composites and Inflatable Structures Structural Membranes 2015*. CIMNE; 2015.
100. Maisner M, Gebhardt M, Gabrys U, Maurer A, Schweizerhof K. Schlauchwehre, Untersuchungen zum Widerstand der Schlauchmembran gegen Beschädigungen. 35. Dresdner Wasserbaukolloquium 2012, "Stahlbauwerke-Planen, Bauen, Betreiben", Proceedings TU Dresden, Dresdner Wasserbauliche Mitteilungen 47. Dresden: Technische Universität Dresden, Institut für Wasserbau und technische Hydromechanik. 2012 47:441-451 (in German).

How to cite this article: Schweizerhof K, Konyukhov A. Some remarks on load modeling in nonlinear structural analysis–Statics with large deformations–Consistent treatment of follower load effects and load control. *Int J Numer Methods Eng*. 2024;e7442. doi: 10.1002/nme.7442